Multifrequency Electron Spin Resonance Study of the Dynamics of Spin Labeled T4 Lysozyme

Ziwei Zhang,[†] Mark R. Fleissner,[‡] Dmitriy S. Tipikin,[†] Zhichun Liang,[†] Jozef K. Moscicki,[†,§] Keith A. Earle,[†,||] Wayne L. Hubbell,[‡] and Jack H. Freed*[,†]

Department of Chemistry and Chemical Biology, Cornell University, Ithaca, New York 14853, Jules Stein Eye Institute and the Department of Chemistry and Biochemistry, University of California, Los Angeles, California 90024, Smoluchowski Institute of Physics, Jagiellonian University, Reymonta 4, PL-30-059 Krakow, Poland, and Department of Physics, University of Albany, SUNY, Albany, New York 12222

Received: November 6, 2009; Revised Manuscript Received: March 2, 2010

An extensive set of electron spin resonance spectra was obtained over a wide range of frequencies (9, 95, 170, and 240 GHz) and temperatures (2 to 32 °C) to explore the dynamic modes of nitroxide-labeled T4 lysozyme in solution. A commonly used nitroxide side chain (R1), or a methylated analogue with hindered internal motion (R2), was substituted for the native side chain at solvent-exposed helical sites, 72 or 131. The spectra at all four frequencies were simultaneously fit with the slowly relaxing local structure (SRLS) model. Good fits were achieved at all the temperatures. Two principle dynamic modes are included in the SRLS model, the global tumbling of the protein and the internal motion consisting of backbone fluctuations and side chain isomerizations. Three distinct spectral components were required for R1 and two for R2 to account for the spectra at all temperatures. One is a highly ordered and slow motional component, which is observed in the spectra of both R1 and R2; it may correspond to conformers stabilized by interaction with the protein surface. The fraction of this component decreases with increasing temperature and is more populated in the R2 spectra, possibly arising from stronger interaction of the nitroxide ring with the protein surface due to the additional methyl group. The other two components of R1 and the second component of R2 are characterized by fast anisotropic diffusion and relatively low ordering, most likely corresponding to conformers having little or no interactions with nearby residues. Ficoll of different concentrations was added to increase the solution viscosity, thereby slowing down the global tumbling of the protein. A significant effect of Ficoll on the internal motion of an immobilized component was apparent in R2 but not in R1. The ability of such multifrequency studies to separate the effects of faster internal modes of motion from slower overall motions is clearly demonstrated, and its utility in future studies is considered.

Introduction

Electron spin resonance (ESR) has been widely used in the study of protein dynamics.[1−8] Protein motions over the 10^{-6} to 10^{-12} s time scales can be investigated by continuous-wave ESR spectroscopy at various frequencies.[9−11]

ESR spectra at different microwave frequencies are sensitive to motions at different time scales. ESR at lower frequencies is more sensitive to the slower motions, whereas ESR at higher frequencies is more sensitive to the faster motions.[12] That is, the slower motions, easily observed in the low frequency ESR spectra, may be frozen at the high frequency time scale. On the other hand, the faster motions, completely averaged out in the low frequency ESR spectra, can be well-resolved at the high frequency time scale. Therefore, multifrequency ESR spectroscopy enables one to separate various motional modes in a protein according to their time scales.[12] Another virtue of the multifrequency ESR approach is the ability to determine accurately the magnetic tensors (the hyperfine (**A**) tensor and **g** tensor) from the rigid limit spectra.[13] High frequency ESR provides greater **g** tensor resolution, because the electron spin Zeeman interaction term becomes dominant in the Hamiltonian at very high frequencies, whereas, the **A** tensor components can be more precisely measured from ESR spectra at low (or conventional) frequencies (∼9 GHz). Until now, ESR at only two frequencies has been used to study the dynamics of proteins.[14−18]

In this paper, we report the results of a more extensive multifrequency ESR approach, covering four frequencies, to study the dynamics of a nitroxide side chain in T4 lysozyme (T4L). T4L is a globular protein composed of 164 amino acid residues with a molecular weight of 18 700 Da. For ESR spectroscopy, a nitroxide spin label is covalently attached to T4L by site-directed spin labeling (SDSL).[1] In SDSL, a cysteine residue is introduced at the site of interest by site-directed mutagenesis and modified with a nitroxide reagent (MTSSL) to generate the spin-labeled side chain designated as R1;[19] the structure of R1 is shown in Figure 1.[5] The motion of the nitroxide can be decomposed into a variety of dynamic modes including the global tumbling of the protein, backbone fluctuations and conformational transitions of the side chain.

For T4L, the slow global tumbling appears frozen at high frequency (e.g., 240 GHz) but affects the low frequency (∼9 GHz) spectra. In contrast, the faster dynamic modes, i.e., backbone fluctuations and side chain isomerizations, affect spectra at both low and high frequencies. The slowly relaxing

* To whom correspondence should be addressed.
[†] Cornell University.
[‡] University of California.
[§] Jagiellonian University.
[||] University of Albany, SUNY.

10.1021/jp910606h
Published on Web 04/02/2010

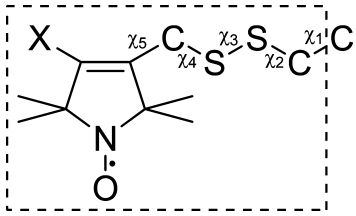

Figure 1. Structure of the R1 (R2) side chain. X = H for R1 (MTSSL), X = CH_3 for R2 (4-methyl-MTSSL).

local structure (SRLS) model was developed to decompose the global tumbling of the protein, and the internal motion consisting of backbone fluctuations and side chain isomerizations.[12,20] In this model, the reorientation of the spin label is restricted by its local environment that relaxes on a longer time scale.[12] ESR spectra recorded at the several frequencies are fit simultaneously using the SRLS model with a common set of dynamic and ordering parameters, which include the overall rotational diffusion tensor of the protein ($\mathbf{R}^c$), as well as the rotational diffusion tensor ($\mathbf{R}^o$) and the order parameters (S_{20} and S_{22} derived from the orienting potential) for the internal motion. In addition, the SRLS analysis allows for the existence of several components in the spectrum, which can, for example, represent several distinct conformers. The multifrequency approach does supply adequate experimental data for reliably determining these fitting parameters.

To explore the dynamics of the spin label linked to T4L at two solvent-exposed helical sites, 72 and 131, we collected well over 200 multifrequency ESR spectra at 5 °C intervals over a temperature range of 2 to 32 °C, out of which we subjected the spectra at 10° intervals (i.e., 2, 12, 22, and 32 °C) to detailed analysis. Compared to our previous two-frequency study on these two sites of T4L,[16] we made the following improvements: (1) We extended the multifrequency study to four frequencies consisting of 9, 95, 170, and 240 GHz; (2) care was taken to ensure that the spectra taken at all four frequencies, necessarily on several spectrometers, were on the same sample and at the same temperature; (3) the newer and improved high frequency ESR spectrometers utilized in this study provided order-of-magnitude improvement in signal-to-noise over the previous study and thereby enabled more reliable spectral fitting, especially with respect to distinguishing more than one spectral component; (4) an additional nitroxide spin label, R2 (also designated as R1b in earlier literature[5]) with structure shown in Figure 1, was also used in order to constrain conformational transitions of the side-chain, enabling contributions from any backbone fluctuations to be enhanced; (5) to better distinguish between the slower global tumbling and the faster internal motion, samples containing different concentrations of Ficoll, which increases the solution viscosity, thereby slowing down the global tumbling of the protein, were also studied.

We simulated this extensive set of experimental spectra with the SRLS model and good fits were achieved to all the data. The analysis of the fitting parameters, in addition to comparing our results with previous studies, provided further insight into the various dynamic modes of T4L.[5,19,21−24] The main findings are the following: (1) For R1, three components could be distinguished, particularly at low temperatures. Liang et al. could not simultaneously fit the 9 and 250 GHz spectra of R1 at or below room temperature using the same set of parameters.[16] They utilized a two-component fit and required different fractional amounts at the two frequencies. We show in the present work that by including the three components in the fitting we can simultaneously fit all spectra at the four frequencies with the same parameters. (2) For R2, just two components may be discerned. One of the two components, highly ordered and with slow isotropic $\mathbf{R}^o$, is also present in R1′s spectra. The fraction of this component for R2 is higher than it is for R1, ostensibly because the interaction of the nitroxide ring with the protein surface is stronger in the case of R2 due to the additional 4-methyl group. (3) A comparison between the results for 72R1 versus 131R1 and 72R2 versus 131R2 suggests that differences in internal modes, in addition to any differences in backbone dynamics, could contribute to the differences between R1 motion at these sites.[5] (4) Values of R^c obtained from our spectral analysis are consistent with the estimates from hydrodynamic theory and NMR experiments. (5) We found in Ficoll solution that the global tumbling is reduced as expected, but the internal motion of an immobilized component for R2, but not R1, is also slowed down somewhat.

Experimental Section

Four nitroxide labeled T4L mutants, 72R1, 131R1, 72R2 and 131R2, were prepared and purified according to methods previously described.[25] The concentration of protein in each sample was between 1 and 2 mM. Ficoll 70 was purchased from Amersham Biosciences (now GE Healthcare Life Sciences) and was used without further purification.

The 9 GHz ESR spectra were obtained on a commercial Bruker spectrometer at a frequency of 9.34 GHz. High-field ESR spectra were obtained on home-built spectrometers.[26,27] The microwave frequencies for the 95, 170, and 240 GHz spectrometers were calibrated, respectively, to be 95.00, 171.10, and 236.64 GHz.

Substantial efforts were made to ensure that the multifrequency data collected on the different spectrometers were consistent. First, the same sample was used in experiments performed on spectrometers at all frequencies. Seventeen millimeter diameter quartz coverslips (ESCO products) were used as sample holders. About 2 μL of sample was placed between a flat quartz coverslip and an etched quartz coverslip with a circular concavity in the middle. The diameter of the concavity to hold the sample is about 1 cm. A thin layer of vacuum grease (Dow Corning) was applied on the edge to create a seal between the two coverslips. Such a sample holder was discussed in detail elsewhere.[28] This same sample and sample-holder was utilized for all three high frequencies. For most experiments performed at 9 GHz it was more convenient to use samples of identical solutions, but sealed in glass capillaries. However in these cases, we first compared the room temperature 9 GHz spectra of the sealed glass-capillary samples with those taken at 9 GHz with the quartz-plate samples utilized at high frequencies. We confirmed that samples in these two types of sample holders yielded identical spectra. For the glass capillary samples, 5 μL of solution was placed in a 0.8 mm i.d. capillary, which was then sealed with fast epoxy.

The temperature at the sample was well calibrated on all spectrometers. To calibrate the temperature for samples placed between quartz coverslips a very thin copper-constantan thermocouple was incorporated into the aqueous sample through the vacuum grease; for the sample sealed in the glass capillary, a copper-constantan thermocouple was placed outside the capillary in the airflow and very close to the sample. The accuracy of the temperature was within ±1 °C. To avoid line shape distortion, we paid special attention to ensure that at each frequency (1) the modulation amplitude was low enough by reducing it sufficiently to levels such that the complex lineshapes are clearly unaffected; (2) the time constant was small enough

TABLE 1: The Nitroxide Labeled T4 Lysozyme Samples for Multifrequency ESR Study in Water and Ficoll Solutions

sample no.	mutant site	spin label	Ficoll concentration (w/v %)	frequency (GHz) 9	95	170	240
1	72	R1	0	√[a]	√	√	√
2	131	R1	0	√	√	√	√
3	72	R2	0	√	√	√	
4	131	R2	0	√	√	√	√
5	131	R1	25	√			√
6	72	R2	15	√	√	√	
7	72	R2	25	√	√	√	
8	131	R2	15	√	√	√	
9	131	R2	25	√	√	√	√

[a] A √ indicates the ESR spectrum has been recorded.

relative to the field sweep rate; and (3) the microwave power was low enough to prevent saturation. The phase of the experimental spectra at 95, 170, and 240 GHz was adjusted to correct for a small admixture of dispersion signal, according to the procedure described previously.[29] The field sweeps of the high frequency spectrometers were calibrated utilizing a standard sample of PD-Tempone in 85% glycerol/H_2O.[30]

Multifrequency ESR spectra of the nine samples listed in Table 1 taken at 2, 12, 22, and 32 °C were utilized for further study.

Additional experiments were performed at low temperatures and high viscosities mainly to obtain accurate rigid limit magnetic tensors, but also to study residual protein motions at the low temperatures. The 9 and 170 GHz spectra of the four mutants were recorded at −50, −35, −20, −5, and +10 °C in 65 w/w% sucrose solution. Samples were prepared by mixing 79 w/w% sucrose and protein solution. To achieve the same final concentration of sucrose in all samples, the same stock solution of 79 w/w% sucrose was used. For experiments at temperatures below the freezing point of 65 w/w% sucrose solution (−17 °C),[31] the sample was initially cooled to −70 °C, and then the temperature was increased to the final temperature.[32] Such an annealing process was applied to produce maximally freeze-concentrated samples at each temperature set point so that at equilibrium the concentration of sucrose was the same in all samples.

Methods

Magnetic Tensor Components. The 9 and 170 GHz spectra of the four mutants in 65 w/w% sucrose solution at −50 °C were simulated to obtain the hyperfine (**A**) tensor and **g** tensor components. Experiments at temperatures lower than −50 °C were also performed at both frequencies (−90 °C at 9 GHz and −155 °C at 170 GHz), but they showed no further change in line shape from those taken at −50 °C. Thus, at −50 °C and in 65 w/w% sucrose solution, the spin label can be regarded as completely immobilized on the time scales of ESR at both frequencies. The 9 and 170 GHz spectra recorded at −50 °C in 65 w/w% sucrose solution displayed identical spectra to those in 30 w/w% Ficoll solution at the corresponding temperature, indicating that the addition of sucrose to 65 w/w% does not affect the magnetic tensor components, considering the different concentrations of sucrose and Ficoll as well as the large difference in their molecular sizes. Timofeev et al.[33] previously found that the isotropic hyperfine constant remains unchanged with the addition of sucrose up to 65 w/w%. These spectra were simulated as rigid limit spectra by performing nonlinear least-squares (NLLS) fits using the microscopic ordering with macroscopic disordering (MOMD) model with an extremely slow motional rate of 10^5 s^{-1}, that is, the rigid limit on the ESR time scale.[34] Magnetic tensor parameters (cf. Supporting Information for details of fitting) are given in Table 2. They are the same for the four mutants within the uncertainty of the experiments and fits. The values of magnetic tensor components, especially of A_{zz} and g_{xx}, are related to the structure of the spin label and the polarity of the local environment to which the spin label is exposed.[35,36] Thus, we find that sites 72 and 131 are exposed to local environments of the same polarity.

TABLE 2: Magnetic Tensor Components[a,b]

mutant site	spin label	g_{xx}	g_{yy}	g_{zz}	A_{xx}	A_{yy}	A_{zz}
72	R1	2.00839	2.00615	2.00232	6.2	4.3	36.9
131	R1	2.00841	2.00616	2.00232	6.0	4.1	37.0
72	R2	2.00841	2.00616	2.00231	6.3	4.6	37.2
131	R2	2.00840	2.00615	2.00231	6.3	4.6	37.1

[a] The estimated absolute error in the **g** tensor components is $\pm 7 \times 10^{-5}$, but the estimated error in their relative values is $\pm 1 \times 10^{-5}$. [b] The estimated error in **A** tensor components is ±0.2 G.

Once determined, the **A** and **g** tensor components were fixed and used as input parameters in the other simulations to extract information regarding dynamic and ordering parameters.

Multifrequency Fitting Using the Slowly Relaxing Local Structure (SRLS) Model. NLLS fits were performed to simulate the multifrequency spectra of the nine samples listed in Table 1 at temperatures from 2 to 32 °C using the fitting program based on the SRLS model. Two dynamic modes of T4L, the global tumbling and the internal motion, are separated in the SRLS model. Rotational diffusion tensors for these two modes are represented respectively by $\mathbf{R^c}$ (global) and $\mathbf{R^o}$ (internal). The theoretical foundation for this model, the definitions of fitting parameters and the fitting procedures are described elsewhere.[16] Fitting parameters, including rotational diffusion tensors $\mathbf{R^c}$ and $\mathbf{R^o}$, potential coefficients (c_{20} and c_{22}), a structural parameter (β_d), and the Lorentzian broadening **W** are obtained from the best fits. Spectra at different frequencies were fit simultaneously. That is, the same set of fitting parameters was used to fit the spectra at all four frequencies, except that **W** the residual width (taken as isotropic W) is allowed to be different at the different frequencies. The observed frequency dependence of W is likely due to random local variations in aqueous polarity which affect the **g** and **A** tensors, with the role of the former increasing with frequency.[14,16,24,30,36]

Four coordinate frames are introduced for the simulation. The first is the magnetic tensor frame, in which the **A** and **g** tensors are defined. For most nitroxide spin labels, the three principal axes of the **A** tensor and the **g** tensor coincide,[37,38] and our rigid limit simulations at 9 and 170 GHz are consistent with this. Thus, the Euler angles between the **A** tensor frame and the **g** tensor frame were set to zero in all simulations. The x-axis is parallel to the N−O bond of the nitroxide and the z-axis is parallel to the p^z orbital of the nitrogen. The second axis frame is the internal diffusion frame for the rotational motion of the spin label tether (including possible local backbone motions). The diffusion of the tether may be taken to be axially symmetric around the z-axis, a matter discussed further below. Thus, the rotational diffusion tensor components, R^o_x, R^o_y and R^o_z, become $R^o_x = R^o_y = R^o_\perp$ and $R^o_z = R^o_\parallel$. The three Euler angles (α_d, β_d, and γ_d) that describe the transformation between the internal diffusion frame and the magnetic tensor frame (i.e., diffusion tilt angles), are related to the conformation of the nitroxide label tether.[34] Among the three diffusion tilt angles, β_d is the angle between the main (z) axis of the internal diffusion frame and

the z-axis of the magnetic tensor frame and is used as a fitting parameter. Given the assumed axial symmetry of $\mathbf{R}^o$, $\alpha_d = 0$, and γ_d is set to zero for convenience.[16]

The orienting potential for the diffusion of the tether is referred to the third axis system, the internal director frame, which is taken as axially symmetric for convenience. The reorientation of the spin label tether is restricted by interaction with its local environment, and the tether tends to align itself into the direction of minimum potential energy. The principal axes of alignment of the spin label tether are taken as coincident with the internal diffusion frame, again for convenience. The degree of restriction of the local motion is characterized by the order parameter S_{20}, and S_{22} measures the asymmetry of this ordering (i.e., its nonaxiality). S_{20} and S_{22} are obtained from the coefficients (c_{20} and c_{22}) in the expansion of the local potential energy function. The fourth coordinate frame is for the tumbling of the protein and is defined as the global diffusion frame. The tumbling of T4L is assumed to be isotropic with no orienting potential for the tumbling. The assumption of isotropic $\mathbf{R}^c$ has been found to be acceptable in a NMR study on T4L.[39]

The presence of more than one component, that is, two or three components, is allowed in the nonlinear least-squares (NLLS) fitting. Further details on the NLLS fitting are given in the Supporting Information.

Results

The Results is divided into three parts. The first part describes the fits to spectra of the four mutants in aqueous solution recorded from 2 to 32 °C. The second part gives the results in 15 and 25 w/v % Ficoll solutions. The temperature range studied in this part is the same as in the first part. In the third part, dynamic information extracted from spectra of the four mutants in 65 w/w% sucrose solution over a temperature range of −50 to 10 °C is described.

Part 1: Analysis of Spectra Recorded in Aqueous Solution. The experimental data and the best fits to spectra of the four mutants in water solution (samples 1 to 4 in Table 1) collected at 2, 12, 22, and 32 °C are displayed in Figure 2, and the best fit parameters are shown in Figure 3 and are listed in Supporting Information Table 1. The diffusion tilt angle (β_d) for each mutant was set to the value listed in the caption for Figure 3 after having been determined as described below. As shown in Figure 2, very good agreement is obtained between the experimental data and the simulations. We first summarize the main features revealed from the fitting.

For R1, three components with different dynamic and ordering parameters for the internal motion were needed in most cases (cf. Figure 3). On the basis of their mobilities, they are referred to as the (relatively) "immobile component", the "intermediate component", and the (relatively) "mobile component", which respectively correspond to components 1, 2, and 3 in Supporting Information Table 1. The immobile component has almost isotropic rotational local diffusion with $R^o_\perp$ similar to $R^o_{||}$. This component is characterized by a higher ordering and a much slower $R^o_\perp$ when compared to the other two components. Unlike the immobile component, the local rotational diffusion of the intermediate and the mobile components is highly anisotropic, with $R^o_\perp$ more than an order of magnitude larger than $R^o_{||}$. The values of $R^o_\perp$ in these two components are about 7 to 14 times those in the immobile component. The mobile component, as compared to the intermediate component, has comparable rotational diffusion rates but much lower ordering.

For R2, the spectra were satisfactorily fit to the superposition of two spectral components. The mobilities of these two components are comparable to those of the immobile and the intermediate components of R1. Thus, for consistency, the two components of R2 are also referred to as the immobile component and the intermediate component. For the intermediate component of R2, $R^o_\perp$ is about an order of magnitude larger than $R^o_{||}$, and the values of $R^o_\perp$ are about 4 to 8 times those of the immobile component. For all the components of R1 and R2, S_{20} remains almost constant over the whole temperature range. The immobile spectral components of the four mutants have similar lineshapes, whereas the mobilities of the intermediate and the mobile components are mutant-dependent. The best fit results for the four mutants are described in detail below.

1. Simulations of Spectra of 72R1. We found that the multifrequency spectra of 72R1 recorded at either 2 or 12 °C could not be simultaneously fit with just one or two components using the same set of fitting parameters. Liang et al.[16] succeeded in fitting these spectra with two components using the same set of fitting parameters, but they required the populations of the two components to be different in the fitting of spectra at different frequencies; they were not able to adequately justify this. The improved S/N, and the fact that four frequencies were used, enabled us to distinguish that in addition to the two components found in the study by Liang et al., a slow motional component (i.e., the immobile component) was discerned in our study. The three peaks corresponding to the immobile component can be observed by eye in the g_{zz} region of the high field spectra (see Figure 4A) with the help of the sensitivity improvement of the spectrometers, whereas these peaks could not be resolved in the previously published 250 GHz spectra.

In fact, some preliminary analyses were performed with two components present in the fitting, an immobile component and a relatively mobile component. However, satisfactory fits cannot be achieved at all frequencies. (1) Two small outer peaks, which are not present in the experimental data, appear in the simulated 9 GHz spectrum (see Figure 4B); (2) The fit to the 240 GHz spectrum is very poor (see Figure 4B). To merge the two outer peaks in the simulated 9 GHz spectrum, we tried to increase the line width or vary R^c in the fitting process, and neither attempt was helpful. The possibility of conformational exchange between the two components was suggested by Liang et al.[16] to address the problem that spectra at 9 GHz and at 250 GHz could not be fitted simultaneously when two components exist. To fit the multifrequency spectra of 72R1 at 2 °C, we tested this idea using a version of SRLS allowing for such exchange, and it was found that the two outer peaks that appear in the simulated 9 GHz spectrum, but which are not observed in the experimental data, were merged when the conformational exchange rate is increased to 6.3×10^7 s^{-1} (see Figure 4C). However, this exchange rate is too slow on the 240 GHz ESR time scale, so that the fit to the 240 GHz spectrum cannot be improved and is still poor. Consequently, the multifrequency spectra of 72R1 at lower temperatures, that is, 2 or 12 °C, could not be simultaneously fit with two components even with conformational exchange included in the simulation.

Thus, in the present study, we allowed the presence of a third component in the simulations. We found consistently that the introduction of another relatively mobile component as the third component leads to good fits at all frequencies. Thus, for example, the two outer peaks in the simulated 9 GHz spectra are merged when three components with different mobilities exist (see Figure 4D). In all, the presence of three components makes it possible to fit spectra at all frequencies with the same set of fitting parameters including the relative populations of the components.

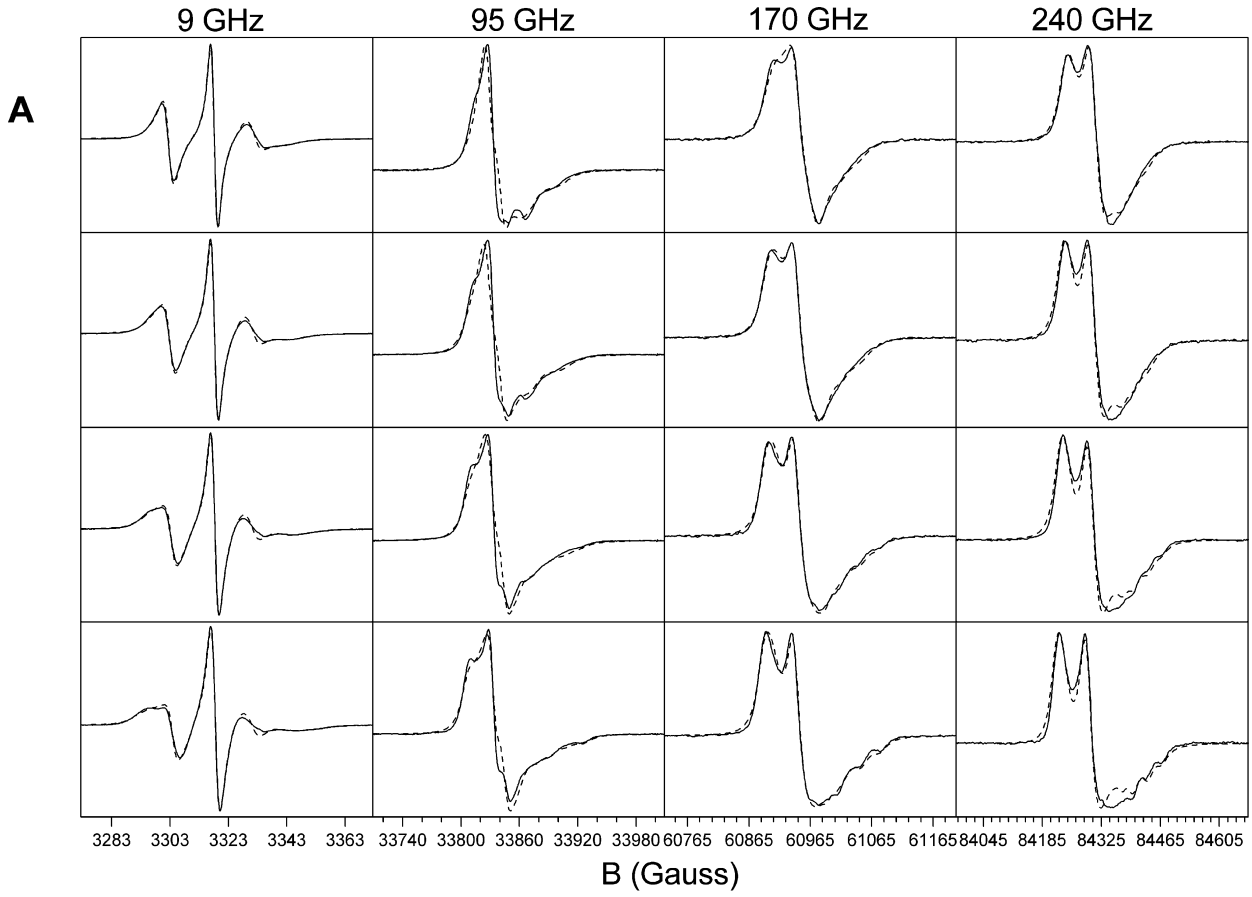

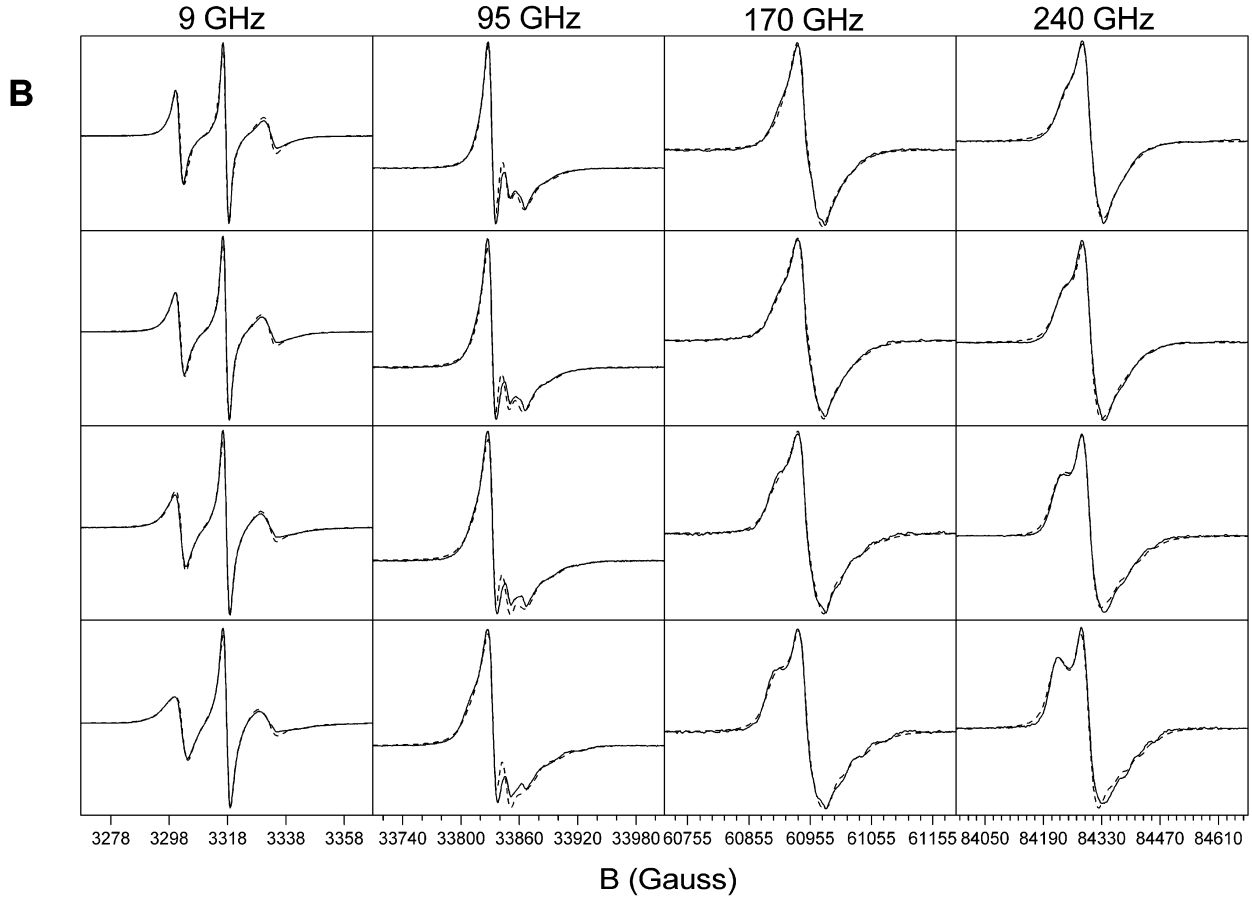

Figure 2. Part 1 of 2.

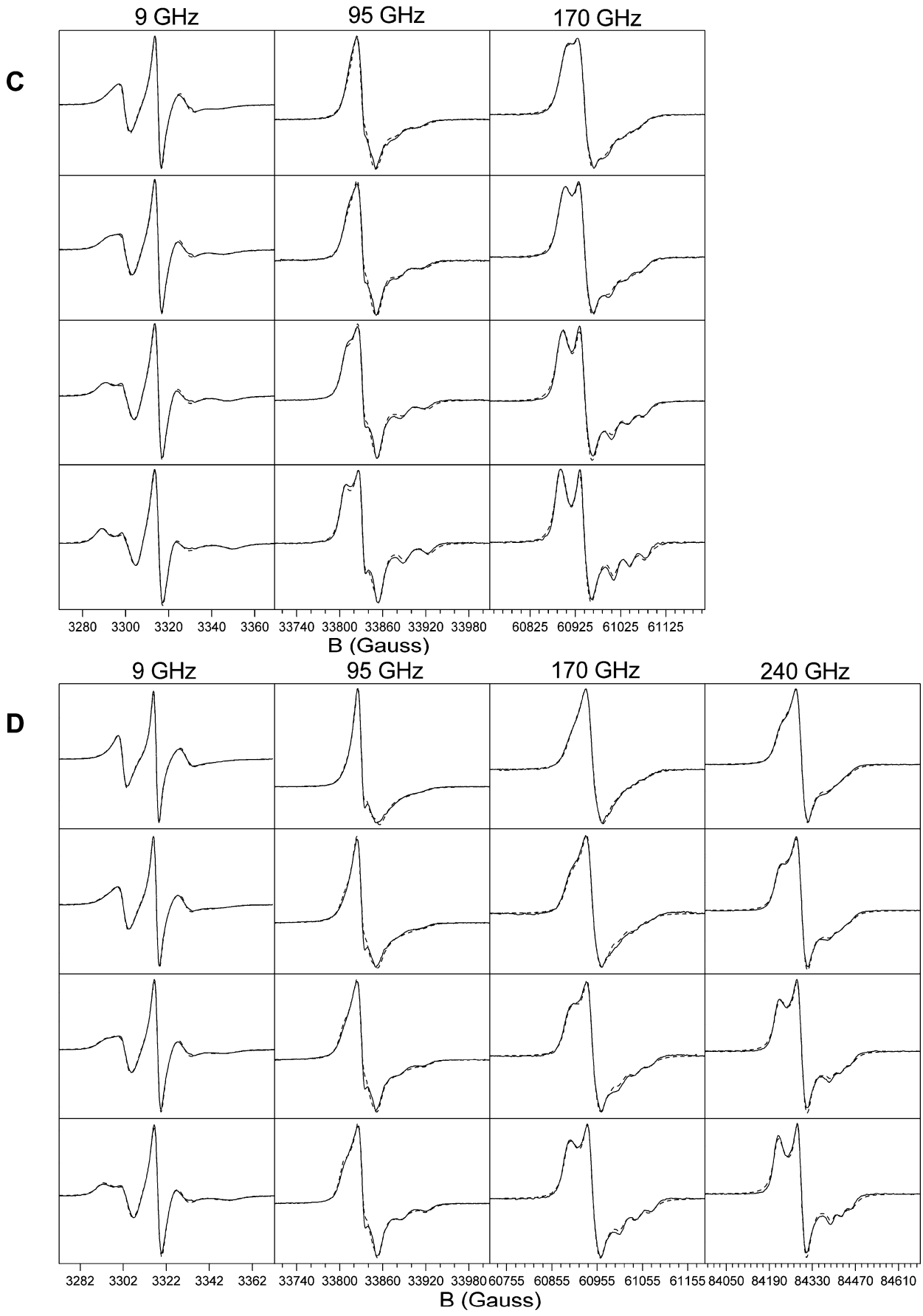

Figure 2. Part 2 of 2. The multifrequency ESR spectra of 72R1 (**A**), 131R1 (**B**), 72R2 (**C**), and 131R2 (**D**) recorded in water solution at 2, 12, 22, and 32 °C (from bottom to top); experimental data (solid line), simulations (dashed line).

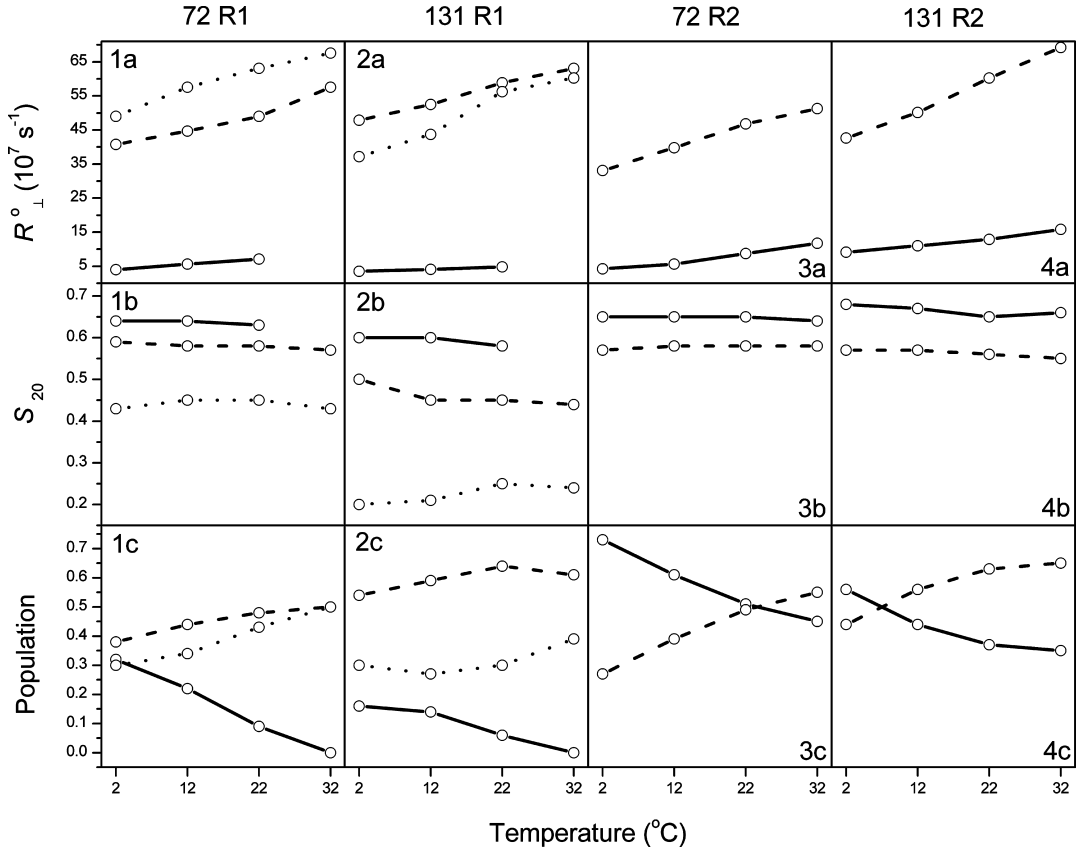

Figure 3. The best fit parameters of $R^o_\perp$, S_{20}, and the relative populations vs temperature from analysis of spectra recorded in water solution; the immobile component (solid line), the intermediate component (dashed line), the mobile component (dotted line). The best fit diffusion tilt angle (β_d) = 21, 20, 30, and 35°, respectively, for 72R1, 131R1, 72R2, and 131R2.

The variation of $R^o_\perp$, S_{20}, and the fractions of the three components with temperature for 72R1 are displayed in subplots 1a−c of Figure 3. At 2 °C, the fractions of the three components are comparable. As the temperature increases, the fraction of the immobile component decreases from 32% at 2 °C to 0% at 32 °C, and the fractions of the intermediate and the mobile components increase. Thus at 32 °C, the spectrum is best fit with just two components with the same population. The immobile component, characterized by the three peaks in the g_{zz} region of the high field spectra, can be observed in the experimental spectra at 95, 170, and 240 GHz, when the temperature is below 22 °C. However, it cannot be observed by eye in the experimental 9 GHz spectra even at 2 °C in aqueous solution. The values of $R^o_\perp$ for the intermediate and mobile components are comparable with that for the former case somewhat smaller at the corresponding temperature, whereas for the immobile component it is nearly an order of magnitude smaller. The values of S_{20} remain almost constant with temperature at 0.64, 0.58, and 0.44, respectively, in the immobile, the intermediate, and the mobile components. The values of S_{22} for the immobile component are very close to zero, indicative of the axial symmetry of the ordering, whereas the values of S_{22} in the intermediate and the mobile components are negative ($-0.31 \sim -0.15$), the implications of which are noted in the next subsection.

2. Simulations of Spectra of 131R1. Similar to 72R1, three components were again required to obtain good fits at all frequencies to the 131R1 spectra (cf. Supporting Information Figure 1). Variations of $R^o_\perp$, S_{20}, and the populations of the three components with temperature for 131R1 are displayed in subplots 2a−c of Figure 3. Over the whole temperature range, the intermediate component is the most abundant with a fraction larger than 50%. As the temperature increases, the fraction of the immobile component decreases from 16% at 2 °C to 0% at 32 °C, whereas those of the intermediate and the mobile components increase. For the immobile component, the value of $R^o_\perp$ is somewhat smaller than that for 72R1 at the corresponding temperature. The values of S_{20} remain almost constant at 0.59, 0.46, and 0.23, respectively, for the immobile, the intermediate, and the mobile components. These are all lower than those of 72R1, especially for the intermediate and the mobile components. The values of S_{22} in the immobile component are very close to zero, whereas the values of S_{22} in the intermediate and the mobile components are respectively negative (−0.21 to −0.15) and positive (0.19 to 0.32). [Note $S_{22} = (2/3)^{1/2}(S_{xx} - S_{yy})$ indicating a switch in the nonaxial preference in ordering from y to x.]

Our results show that the population distributions as well as the rotational diffusion rates at site 72 and site 131 are somewhat different. But, the difference in lineshapes at these two sites is still found to be primarily from the difference in ordering.

3. Simulations of Spectra of 72R2. The 170 GHz spectrum of 72R2 recorded at 2 or 12 °C cannot be satisfactorily fit with only a single component since the spectral features in the g_{zz} region cannot be well reproduced by just a single component (see Supporting Information Figure 2). To reproduce the spectral features at all frequencies, a second component was allowed in the fitting.

Variations of $R^o_\perp$, S_{20} and the populations of the two components with temperature for 72R2 are displayed in subplots 3a−c of Figure 3. The immobile component is the dominant component when the temperature is below 22 °C, whereas it is approximately equal in percentage to the intermediate component when the temperature is at or above 22 °C. For the

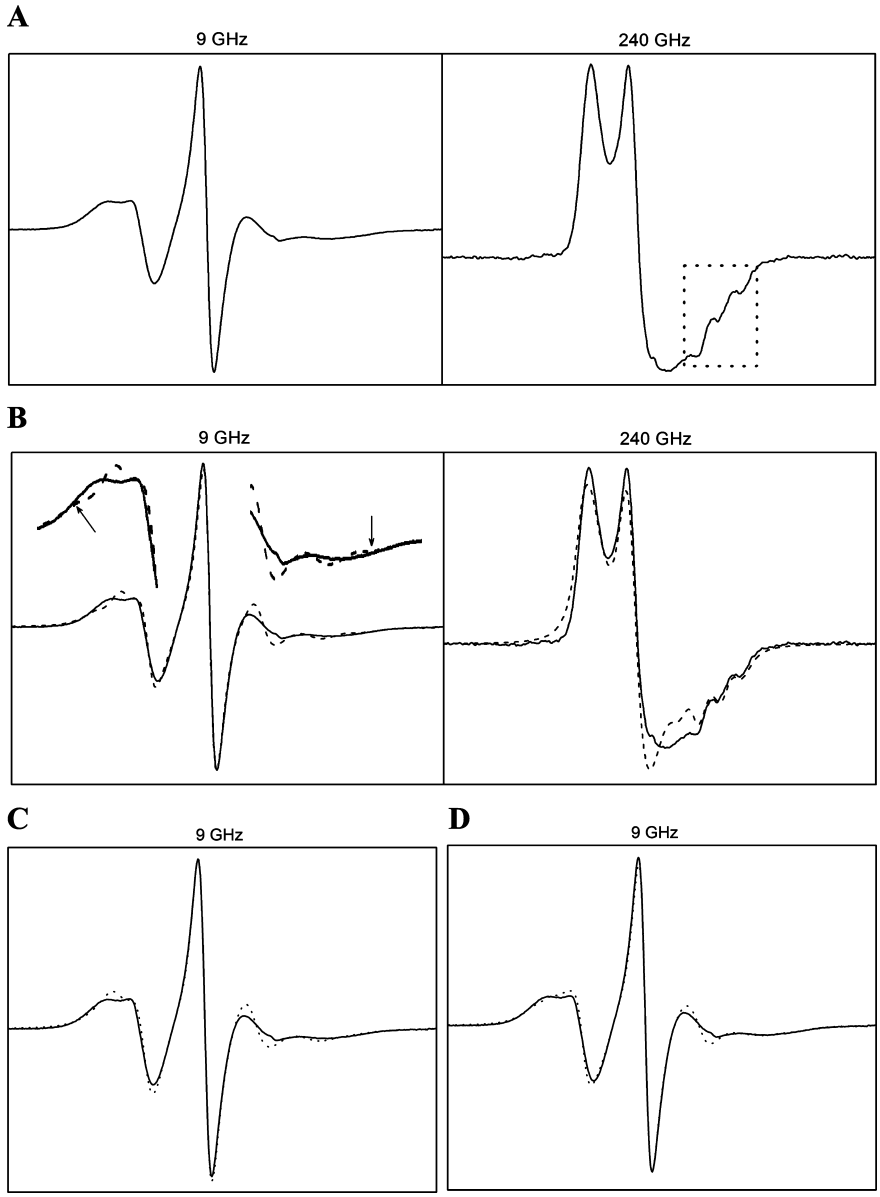

Figure 4. The two-component and three-component fits to the spectra of 72R1 recorded at 2 °C. (A) The 9 and 240 GHz experimental spectra for 72R1 recorded at 2 °C. The dashed rectangle shows the immobile component features that can be observed by eye in the 240 GHz spectrum, but not in the 9 GHz spectrum. (B) The two component fits to the 9 and 240 GHz spectra of 72R1 recorded at 2 °C; experimental data (solid lines), simulations (dashed lines). The arrows point to the two outer peaks present in the two component fit but not in the experimental data. These two outer peaks are merged when the two components exchange with a rate of 6.3×10^7 s^{-1} shown in (C). (D) The three component fit to the 9 GHz spectrum of 72R1 recorded at 2 °C; experimental data (solid line), simulation (dashed line). The outer peaks are not present in the three component fit.

immobile component, the values of $R^o_\perp$ are slightly larger than that of 72R1 at the corresponding temperature. The values of $R^o_\perp$ for the intermediate component are smaller than that of 72R1. The values of S_{20} remain nearly unchanged at 0.65 and 0.58, respectively, in the immobile and the intermediate components. They are almost the same as those of 72R1. The values of S_{22} in the two components are close to zero, indicative of axial symmetry.

On the basis of the fitting results, 72R1 and 72R2 have substantially different population distributions. The immobile component of 72R2 is about 40% more populated than that of 72R1 at the corresponding temperature, as will be discussed below.

4. Simulations of Spectra of 131R2. Similar to 72R2, the 170 and 240 GHz spectra of 131R2 cannot be satisfactorily fit with a single component, since the spectral features in the g_{zz} region at the lower temperatures cannot be well reproduced by just a single component (see Supporting Information Figure 3). Thus, a second component was again added in the fitting. Columbus et al. also found that the 9 GHz spectra of 131R2 in 30% sucrose solution cannot be well fit with a single component using the MOMD model.[5]

Variations of $R^o_\perp$, S_{20}, and the populations of the two components with temperature for 131R2 are displayed in subplots 4a−c of Figure 3. The immobile and the intermediate components are evenly distributed when the temperature is below 22 °C. At and above 22 °C, the intermediate component becomes the more abundant.

Unlike the case of R1, where the mobilities of the intermediate and the mobile components at site 72 differ from those at site 131 mostly in their ordering, 72R2 and 131R2 have similar S_{20} for the intermediate component (0.58 at site 72 vs 0.56 at site 131). Compared to 72R2, the intermediate component of 131R2 has a modestly faster $R^o_\perp$ and is about 15% more abundant.

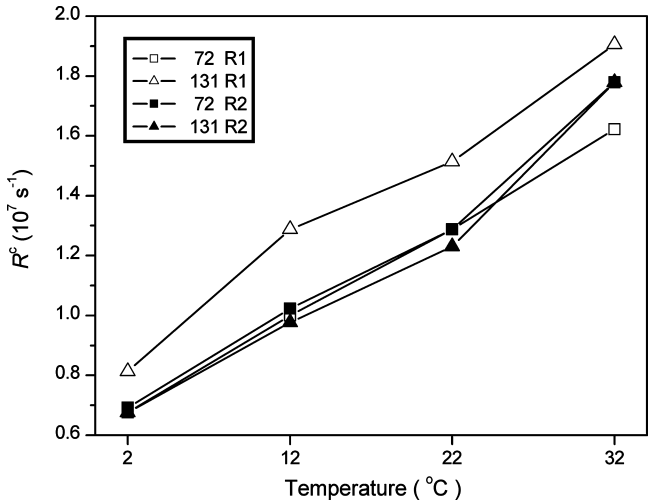

Figure 5. The best fit R^c vs temperature from analysis of spectra recorded in water solution.

TABLE 3: Comparison of the Global Tumbling Rates of T4 Lysozyme from the Multifrequency ESR Fits, from the NMR Estimate, and from the Hydrodynamic Model Calculation

T (°C)	average R^c [a] (10^7 s^{-1})	standard deviation (10^7 s^{-1})	NMR[b] (10^7 s^{-1})	$D_{0,\perp}$[c] (10^7 s^{-1})	$D_{0,\|}$[c] (10^7 s^{-1})
2	0.72	0.06	0.63	0.93	0.59
12	1.07	0.13	0.89	1.31	0.83
22	1.33	0.11	1.19	1.75	1.11
32	1.77	0.10	1.54	2.26	1.43

[a] Average R^c = (R^c of 72R1 + R^c of 131R1 + R^c of 72R2 + R^c of 131R2)/4 (see Supporting Information Table 1 for R^c of 72R1, 131R1, 72R2 and 131R2). [b] Calculated from the NMR result[39] at 10 °C extrapolated using the Stokes−Einstein relation. [c] Calculated from $D_{0,\perp}$ and $D_{0,\|}$ at 25 °C (from Table 1 in ref 22) extrapolated using the Stokes−Einstein relation.

With regard to the population distribution, the comparison between 131R1 and 131R2 is similar to that between 72R1 and 72R2. 131R2 has about 35% higher percentage of immobile component than does 131R1.

5. Additional Aspects: Overall Tumbling, Diffusion Tilt, Nonaxial Internal Diffusion. The temperature dependence of R^c found for the four mutants in aqueous solution is shown in Figure 5. They are very similar with the exception of 131R1, which is about 20% greater. The average of the values for the four mutants and the standard deviations are given in Table 3. Also in this table the average R^c is compared to the value determined by NMR[39] as well as to the diffusion tensor $\mathbf{D_o}$ estimated from a hydrodynamic model on the basis of the crystal structure of T4L.[22] The values for the average R^c are about 10% below the mean $D_o = (2\ D_{o,\perp} + D_{o,\|})/3$, and are about 15% greater than the NMR estimate. These small differences may arise in part from the neglect of the small asymmetry in R^c in the experimental analyses. Note that whereas R^c is varied in the fitting process, it can be fixed to the average value in Table 3 and still good fits can be obtained.

The diffusion tilt angle (β_d), as noted in Methods, is related to the conformation of the nitroxide label tether. The best fit β_d was determined by fitting the most challenging multifrequency spectra, which are those at 2 °C. [A few checks at 22 °C indicated there was not much temperature dependence of β_d.] For each mutant, we performed separate fits to the multifrequency spectra recorded at 2 °C in water solution with β_d fixed to a series of values in the range of 0−40°. Variations of the reduced χ^2 with β_d are plotted in Supporting Information Figure 4. The best fit β_d that yielded the minimum reduced χ^2 was found and listed in the caption for Figure 3 for each mutant. (In the fitting, the β_d was taken as common for all components. To have allowed β_d to vary separately for each component would have introduced too many parameters. However, we do note that the value of β_d only affects the intermediate and fast spectral components but not the slow one.) Subsequently, β_d was fixed at the value in the caption for Figure 3 when fitting spectra recorded at the other temperatures and spectra of the mutants in Ficoll solution. Although different values of best fit β_d were found for the four mutants, these values lie within the range of 20−35°. In a previous study, an angle of 20−30° between the rotation axis of χ_4 and the z-axis of the magnetic tensor frame was derived from an energy-minimized model of the side chain based on the crystal structure.[5] Thus, it would appear that the z-axis of the internal diffusion frame is approximately parallel to the rotation axis of χ_4, as concluded previously from simulation of 9 GHz spectra.[5]

The effect of β_d on the spectrum is an interesting one. Faster internal modes of motion, will partially average an axial magnetic tensor, such as the **A** tensor, so that its effective magnitude is reduced by $|S_{2,0}|[(1/2)(3\cos^2\beta_d - 1)]$, which then must be averaged by the slower overall tumbling.[12] Thus, a value of $\beta_d \sim 30°$ leads to a value of five eighths for the expression in brackets, compared to unity for $\beta_d = 0°$. This means that for $\beta_d > 0°$, the overall tumbling has a reduced effect on the spectrum. This is the case for 9 GHz, which is dominated by the axial **A** tensor, whereas for high frequencies, dominated by the nonaxial **g** tensor, this is somewhat less the case. We find that with a $\beta_d = 0°$, the $R^c_{average}$ values given in Table 3 are increased by about 30%.

In addition, we find that there is some correlation in the parameters for the internal motion with choice of tilt angle, β_d. Thus, if $\beta_d = 0°$ is used for the R1 cases instead of 20°, $R^o_\perp$ is typically only mildly affected, but $R^o_\|$ is increased very substantially for the mobile and intermediate cases (but not for the immobile case), and it is still true that $R^o_\perp \gg R^o_\|$. The effects are more modest using $\beta_d = 0°$ instead of 30−35° for the R2 cases. S_{20} and S_{22} (as well as c_{20} and c_{22}) are only slightly affected in all these cases.

In our work, all the analyses were performed with an axially symmetric internal diffusion tensor $\mathbf{R^o}$ ($R^o_x = R^o_y = R^o_\perp$ and $R^o_z = R^o_\|$) instead of a fully anisotropic $\mathbf{R^o}$ ($R^o_x \neq R^o_y \neq R^o_z$). To verify that an axially symmetric $\mathbf{R^o}$ is sufficient, the multifrequency spectra of the four mutants recorded at 2 °C in aqueous solution were fit with $\mathbf{R^o}$ assumed to be either axially symmetric or fully anisotropic. The fits were found to be only slightly improved with $R^o_x \neq R^o_y \neq R^o_z$. The best results indicate that the average of R^o_x and R^o_y is close to the $R^o_\perp$ for the case of axial symmetry, and R^o_z is close to $R^o_\|$. The other fitting parameters, including the order parameters and the percentages of the multiple components, were unaffected by the assumption of the axial symmetry in $\mathbf{R^o}$. Therefore, to avoid excessive fitting parameters, the internal diffusion tensor was restricted to axial symmetry.

Part 2: Analysis of Spectra Recorded in Ficoll Solution. Ficoll 70 is a macromolecule with an approximate molecular weight of 70 000 Da, which is about 4 times the molecular weight of T4L. Ficoll was added into the aqueous solution in order to increase the viscosity of the solution and slow down the global tumbling of the protein. The experimental and the fitted spectra of 131R1, 72R2, and 131R2 in 15 and 25 w/v % Ficoll solutions (samples 5 to 9 in Table 1) at 2, 12, 22, and 32

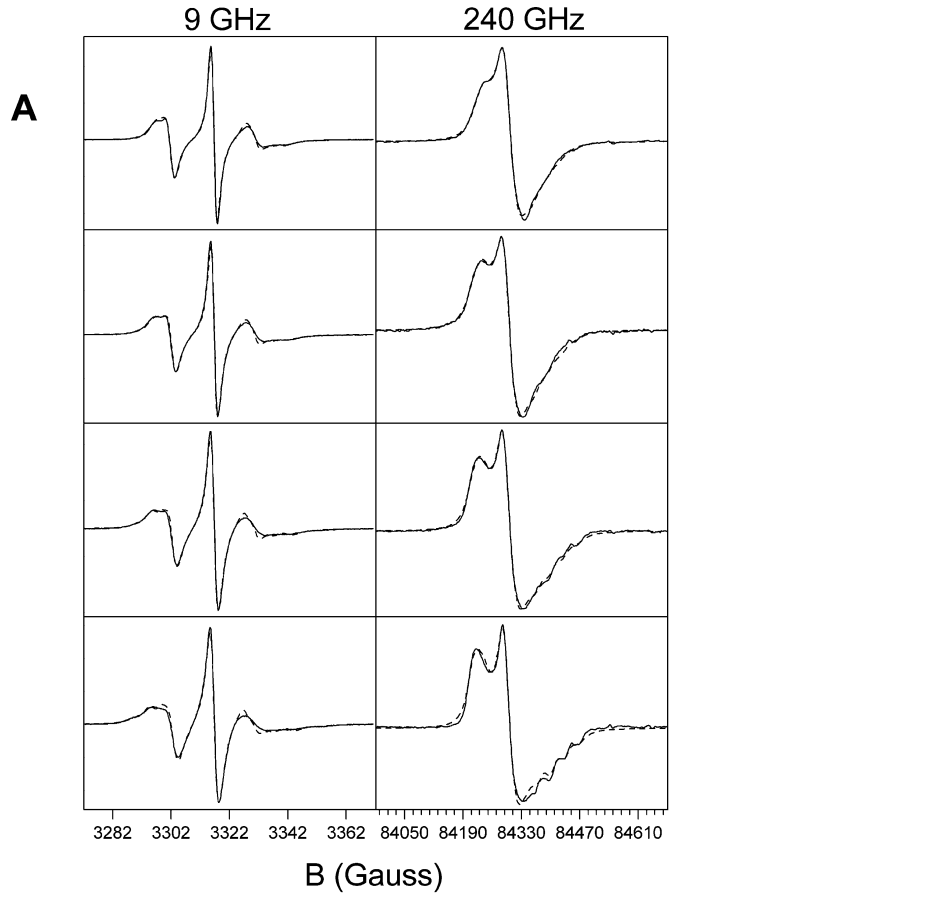

Figure 6. Part 1 of 3.

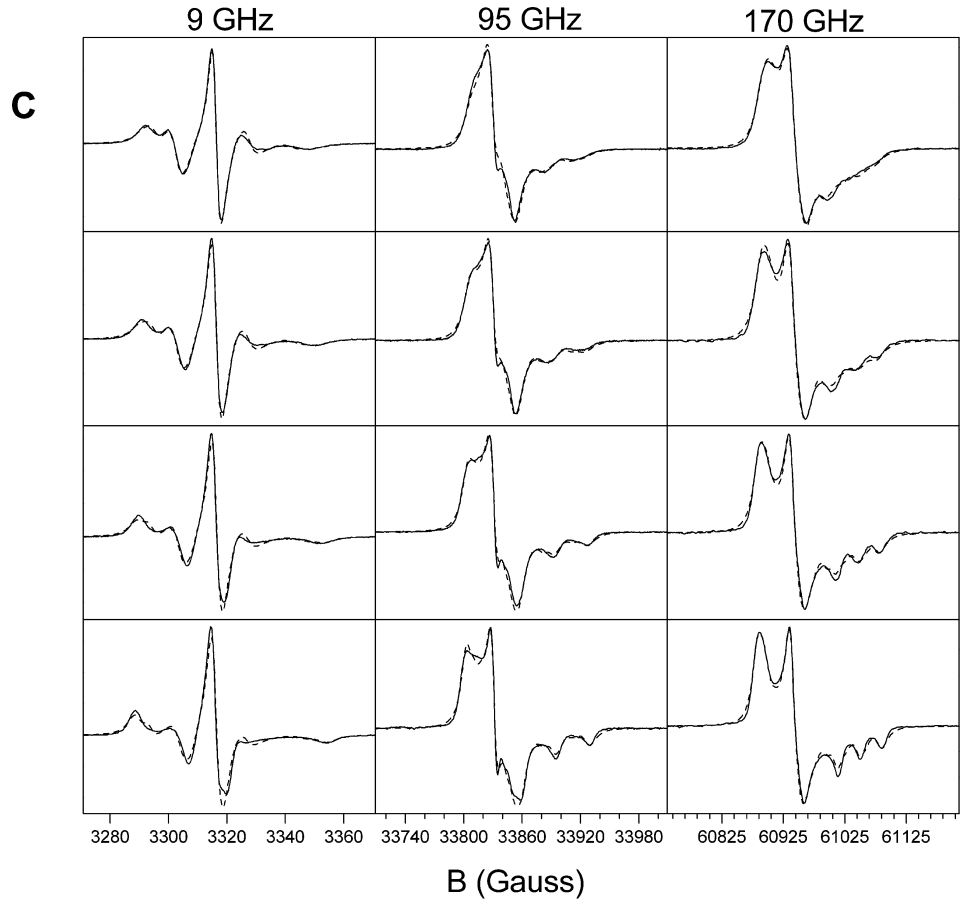

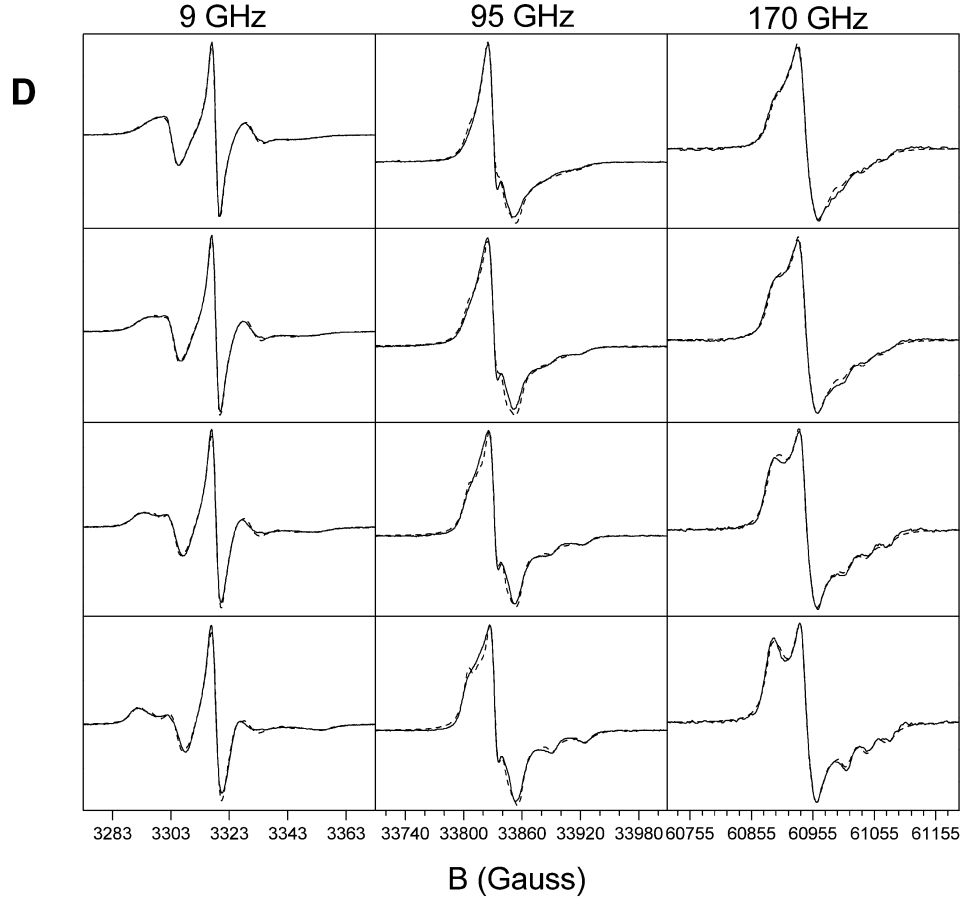

Figure 6. Part 2 of 3.

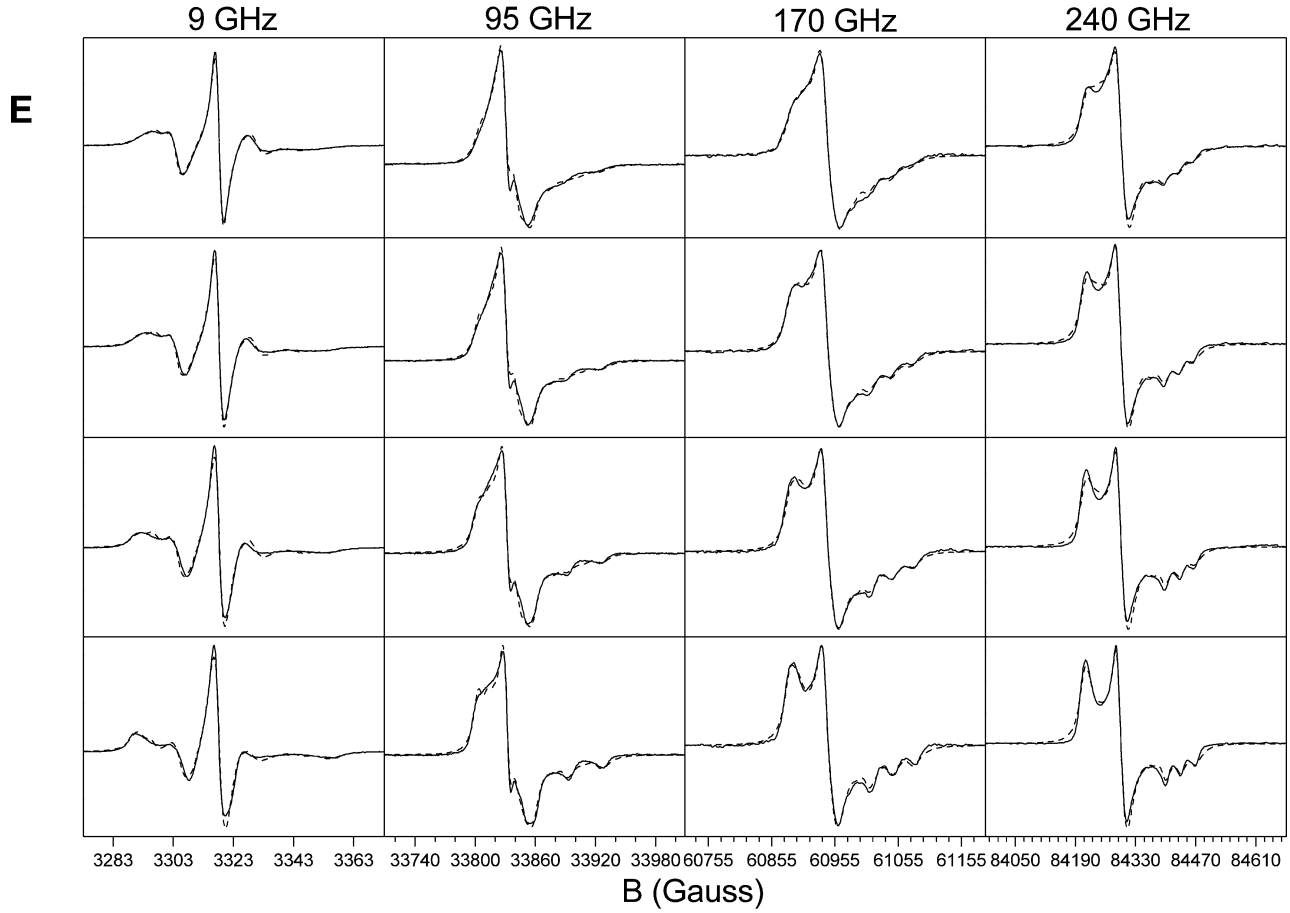

Figure 6. Part 3 of 3. The multifrequency ESR spectra of 131R1 (A), 72R2 (B,C) and 131R2 (D,E) recorded in 15 (B,D) and 25 w/v % (A,C,E) Ficoll solutions at 2, 12, 22, and 32 °C (from bottom to top); experimental data (solid line), simulations (dashed line).

°C are compared in Figure 6, showing good agreement. The best fit parameters are listed in Supporting Information Table 2. The values of $R^{o}_{\perp}$, S_{20}, and the percentages of the components vs temperature in different concentrations of Ficoll solutions are displayed and compared in Figure 7. It is found that the spectra of each mutant in 0, 15, and 25% Ficoll solutions cannot be fit equally well with the same set of internal dynamic and ordering parameters with just different global tumbling rates (R^{c}). Therefore, the spectra with different Ficoll concentrations were fit separately, and the parameters derived from the best fits were compared to determine which are influenced by the addition of Ficoll.

The macroscopic viscosity of Ficoll solution and the microscopic viscosity for the global tumbling of T4L calculated from R^{c} are compared in Table 4. It was shown by Lavalette et al.[40] that the linear viscosity dependence of the Stokes−Einstein relation should be replaced by a power law to describe the rotational diffusion of proteins in a macromolecular environment. This can explain the significant difference between the values of the macroscopic and microscopic viscosities in Table 4. In fact, we find $\eta(\text{micro}) \propto [\eta(\text{macro})]^{0.39}$. The temperature dependence of the microscopic viscosity is shown in Figure 8.

The spectra recorded in Ficoll solution were fit with three components for R1 and with two components for R2. The population distributions are close to those in aqueous solution with any differences within only 10%.

Our results for R2′s motion show that adding 25% Ficoll has little effect on $R^{o}_{\perp}$ of the intermediate component, whereas the ordering (S_{20}) of this component is increased slightly relative to that in water solution. The most notable effect after adding Ficoll is that the value of $R^{o}_{\perp}$ in the immobile component is reduced by 50−60%. The ordering of the immobile component is very slightly increased.

Ratios of rotational diffusion rates in Ficoll solution over those in aqueous solution are shown in Figure 9, clearly displaying the effects of the Ficoll noted above.

For 131R1, the effect of 25% Ficoll on either the intermediate or the mobile component is small, similar to that on the intermediate component of R2. However, contrary to the case of 131R2, both $R^{o}_{\perp}$ and S_{20} change only slightly in the immobile component of R1 when Ficoll is added into the solution. The large decrease in $R^{o}_{\perp}$ as found in R2 is not observed in R1, in general agreement with the results of Lopez et al.[41] Possible explanations for why the internal motion is damped for R2 in Ficoll solution will be discussed below.

Part 3: Analysis of Spectra Recorded in 65 w/w% Sucrose Solution. The 9 and 170 GHz spectra of the four mutants in 65 w/w% sucrose solution were recorded over a temperature range of −50 to 10 °C. The spectra of 72R2 and 131R2 are identical over the whole temperature range (see Figure 10), whereas the spectra of 72R1 and 131R1 have identical lineshapes only at very low temperatures, for example, −50 and −35 °C (see Figure 11). At the higher temperatures, for example, −5 and 10 °C, their spectra are significantly affected by incipient motions; the motion of 131R1 is found to be faster than that of 72R1, as seen in Figure 11. At 10 °C, the identical spectra observed for 72R2 and 131R2 can be fit with just a single component, that is, the immobile component. However, the spectra of 72R1 and 131R1 at 10 °C cannot be well fit with just a single component. In addition to the immobile component, some amount (∼35%) of the intermediate

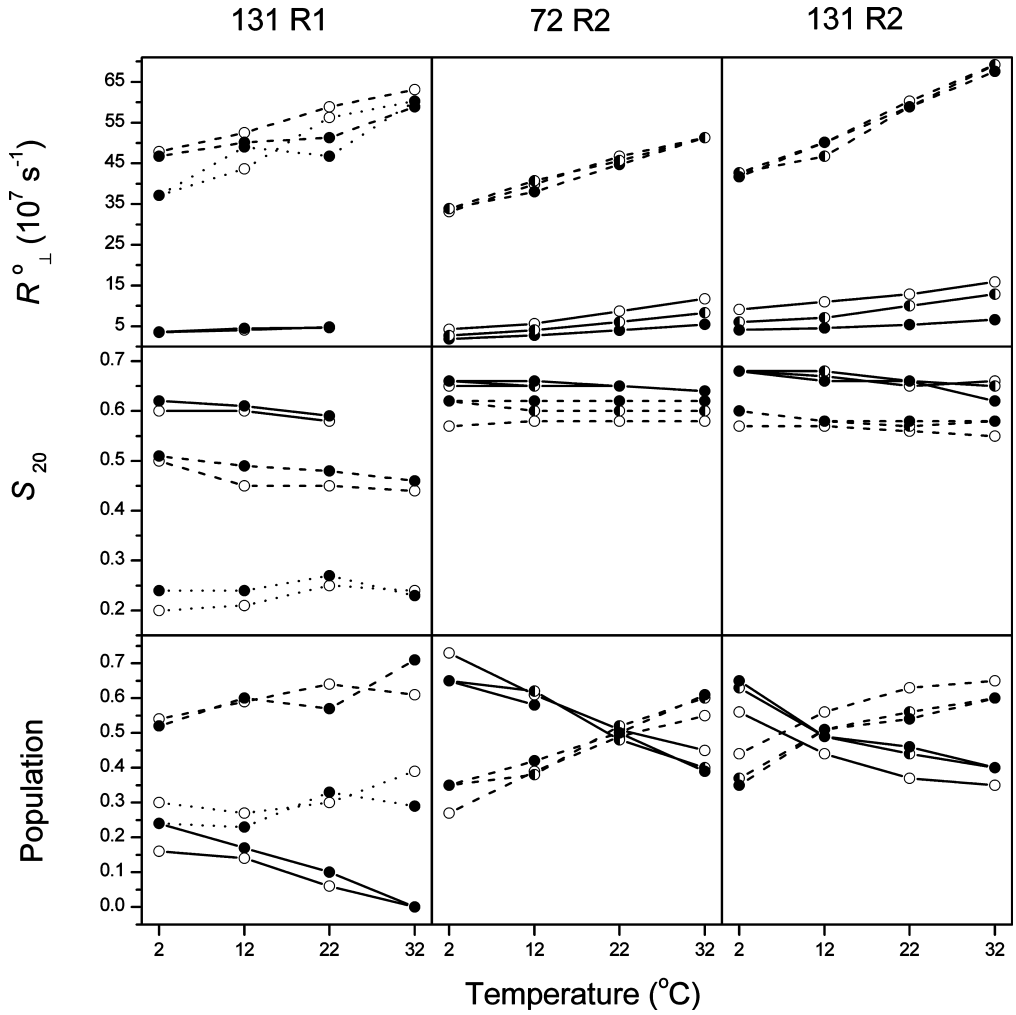

Figure 7. The best fit parameters of $R^{o}_{\perp}$, S_{20}, and the relative populations vs temperature from analysis of spectra recorded in water solution (○), in 15 w/v % Ficoll solution (◐), and in 25 w/v % Ficoll solution (●); the immobile component (solid line), the intermediate component (dashed line), the mobile component (dotted line).

TABLE 4: Comparison of the Macroscopic and the Microscopic Viscosities of 15 and 25 w/v % Ficoll Solutions

Ficoll concentration (w/v %)	macroscopic viscosity at 20 °C[a]	microscopic viscosity at 22 °C[b]
15	5.6	2.05
25	16.6	3.39

[a] Viscosity of solutions of Ficoll 70 relative to that of water from product information sheet provided by Amersham Biosciences (now GE Healthcare Life Sciences). [b] The microscopic viscosity for the global tumbling of T4 lysozyme relative to that in water. Values were determined by dividing R^{c} of 72R2 in water solution (see Supporting Information Table 2).

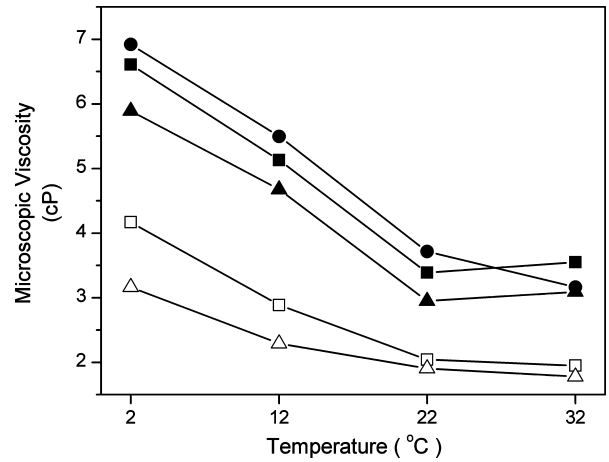

Figure 8. The relative microscopic viscosity with regard to the global tumbling of T4 lysozyme in 15 w/v % (unfilled symbols) and 25 w/v % (filled symbols) Ficoll solutions vs temperature; 131R1 (circles), 72R2 (squares), 131R2 (triangles). Relative microscopic viscosity ≡ R^{c} in water solution/R^{c} in Ficoll solution.

and/or the mobile component still exists, and the difference in the mobilities at these two sites results in the spectra of 72R1 and 131R1 being different. Further discussion of these spectra may be found in the Supporting Information.

At −50 °C, the sample is frozen since the glass transition temperature of the sucrose solution is −40 °C.[31] In the glass, one expects the motions of all components to be extremely slow or frozen, so all spectra are the same for the different spin labels and sites since they have the same magnetic tensors.

Discussion

Comparison with Model of Tombolato et al. One of the results of this work is that we find three components different in their internal mobility when simulating the spectra of R1. One is a highly ordered relatively immobile component, and the other two are relatively weakly ordered components referred to as the intermediate and the mobile components with comparable rotational diffusion rates ($R^{o}_{\perp}$) but significantly

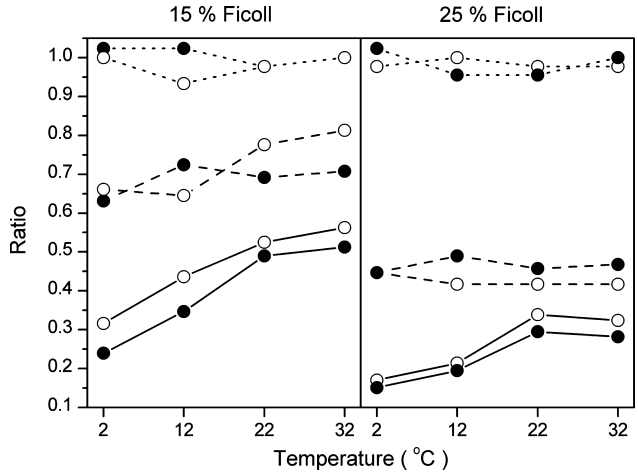

Figure 9. Decrease of R^c (solid line), $R^o_\perp$ in the immobile component (dashed line), and $R^o_\perp$ in the intermediate component (dotted line) of 72R2 (filled circles) and 131R2 (unfilled circles) in 15 and 25 w/v % Ficoll solutions. Ratio ≡ rotational diffusion rate in Ficoll solution/ rotational diffusion rate in water solution.

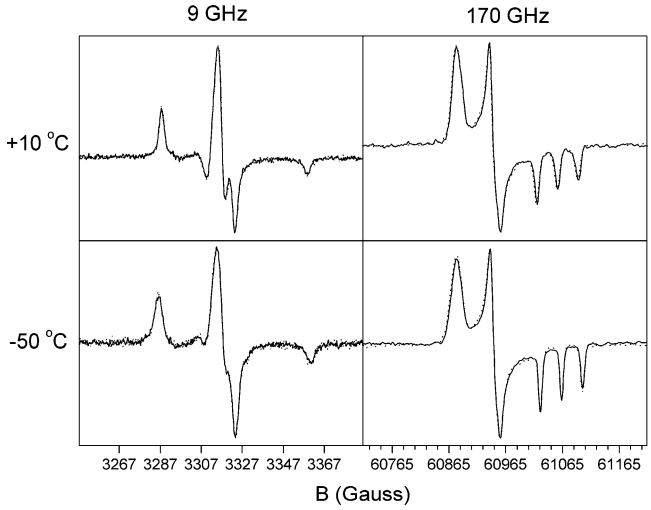

Figure 10. Comparison of spectra of 72R2 (solid line) and 131R2 (dashed line) recorded in 65 w/w% sucrose solution at +10 and −50 °C.

different orderings (S_{20}). The finding of three components in R1′s spectra is in good agreement with a theoretical study of the conformational dynamics of R1 at the solvent-exposed helical site 72 of T4L by Tombolato et al.[22] According to that study, the multicomponent character is an intrinsic feature of the spectra of R1 and at least three components are necessary in the simulation. The values of S_{20} they obtained for their three components were 0.68, 0.52, and 0.37 when simulating the 9 GHz spectrum of 72R1 at 10 °C. Correspondingly, we obtained three components with $S_{20} = 0.64$, 0.58, and 0.45 from the fits to the multifrequency spectra of 72R1 at 12 °C (cf. Supporting Information Table 1). It followed from the conformational dynamics study that the two relatively mobile components originate from the same conformers but with different torsional distributions about the minima in the energy profile for rotation about χ_5.[22] This would explain why the two relatively mobile components that we find differ from each other in ordering.

As noted in Results, the immobile component has almost isotropic $\mathbf{R^o}$ and its mobility is similar at site 72 and site 131. In a previous two-frequency ESR study of T4L dynamics, an immobile component was also found when simulating the spectra of R1 linked to another two solvent-exposed helical sites

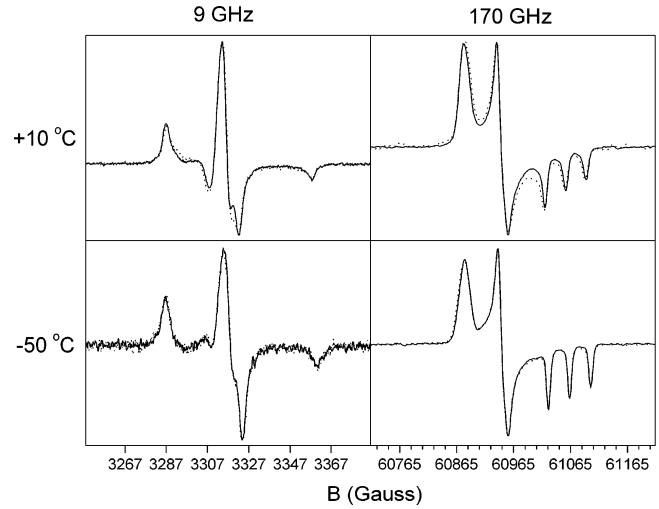

Figure 11. Comparison of spectra of 72R1 (solid line) and 131R1 (dashed line) recorded in 65 w/w% sucrose solution at +10 and −50 °C.

(44 and 69), and its mobility was found to be similar at these two sites as well.[14] The existence of such an immobile component at solvent-exposed helical sites has been ascribed to a weak interaction of the nitroxide ring with the protein surface (Columbus et al.;[5] Fleissner et al.[25]). According to Tombolato et al., the change of spectral line shape with increasing temperature arises from increasing global tumbling and increasing internal mobility of each component, whereas the population of each component remains unchanged.[22] However, our results show that the population of each component does vary with temperature and the population of the immobile component decreases with increasing temperature. Our results are supported by molecular modeling, which suggests that the conformers corresponding to immobile components are entropically unfavored, and a weak interaction is necessary to stabilize them.[23] The interaction is so weak that it exists only at reduced temperature, so that the immobile component becomes more abundant at lower temperatures.[5]

In this study, we discerned two components in the spectra of R2, which, compared to the three components in the case of R1, allow for a simpler description of the dynamics of R2. Tombolato et al. found that the spectrum of 72R2 is composed of similar spectra of a series of conformers, so that the spectrum of R2 can be simulated with a single component.[22] Additionally, they suggested that the spectrum of R2 is not far from a rigid limit spectrum with partially averaged magnetic tensors. Our results indicate that in addition to an immobile component, which yields a spectrum similar to the rigid limit case, a more mobile component, referred to as the intermediate component in this paper, also exists. We found that the spectra of R2 have some features in common with those of R1. (1) There is a highly ordered immobile component; (2) the intermediate component has an anisotropic $\mathbf{R^o}$ and relatively lower ordering. Fleissner obtained the same crystal structure for 131R1 and 131R2.[23] This may help to explain why the spectra of R1 and R2 share such common features.

Effects of Added Methyl Group in R2. Now we wish to discuss the change of spectral line shape when a methyl group substitutes the hydrogen atom at the 4-position of the nitroxide ring of R1, that is, when R2 is linked to the mutant. On the basis of the molecular modeling described by Columbus et al., it was suggested that the 4-substituent increases the ordering because of the steric clash with the disulfide which reduces the

amplitude of rotation about χ_5.[5] This is consistent with our current results that 72R2 and 131R2 have more highly ordered components than 72R1 and 131R1, respectively. For example, the value of S_{20} in the intermediate component of 72R2 is higher than the average of S_{20} in the two relatively mobile components of 72R1. Similarly, the value of S_{20} in the intermediate component of 131R2 is higher than both order parameters in the two relatively mobile components of 131R1. At both sites, the larger population of the immobile component of R2 compared to R1 can be caused by the stronger interaction between R2 and the protein surface because of the additional methyl group.[5] As previously noted,[5] with the 4-methyl group the interaction between the nitroxide ring and its nearby residues is evident in the 9 GHz spectrum of 131R2 recorded at room temperature in 30% sucrose solution, whereas such an interaction cannot be clearly observed in the spectrum of 131R1 at room temperature. Such observations are further confirmed by our quantitative analysis showing that the immobile component, stabilized by such interaction, is more populated in the spectra of R2 than in those of R1.

Comparison of $R^{\circ}_{\perp}$ versus $R^{\circ}_{\|}$. According to our results, it is shown that $R^{\circ}_{\perp} \gg R^{\circ}_{\|}$ in the two relatively mobile components of R1 and in the intermediate component of R2. As noted in Results, $R^{\circ}_{\|}$ is roughly parallel to χ_4, and as noted in ref 5 $R^{\circ}_{\perp}$ is in the plane of the nitroxide ring where χ_5 lies. Liang et al. also observed that $R^{\circ}_{\perp}$ in the dominant component of 72R1 and 131R1 is an order of magnitude larger than $R^{\circ}_{\|}$ in their two-frequency study.[16] Also, Barnes et al. obtained $R^{\circ}_{\perp} > R^{\circ}_{\|}$ by nearly a factor of 10 from their study of 44R1 and 69R1 at 9 and 250 GHz.[14] Such a relation between $R^{\circ}_{\perp}$ and $R^{\circ}_{\|}$ indicates that the rotation about χ_5 is the major contributor to the fast conformational transitions in the relatively mobile components of R1 and R2. That the rotation about χ_5 is the fastest rotation has been shown by studies using various methods by Mchaourab et al., Budil et al., Tombolato et al., and Sezer et al.[19,21,22,24] Moreover, simulation of the 9 GHz spectrum of 41R1 in terms of the MOMD model yielded a mobile component with anisotropic $\mathbf{R}^{\mathbf{o}}$ and an immobile component with isotropic $\mathbf{R}^{\mathbf{o}}$, that is, in general agreement with our observations.[42]

Dynamics at Site 72 versus Site 131. We have shown in our present work that the magnetic tensors determined from the rigid limit spectra (obtained at −50 °C in viscous sucrose/water solution) are identical for the mutants at site 72 and at site 131. Thus it is very likely that the differences in the dynamic spectra observed around room temperature arise primarily from differences in their dynamics. As in past studies we adopt this viewpoint, and we also consider the following. Both sites were defined as solvent-exposed helical sites.[19] It was shown that they have no interaction with their local environment by the fact that their spectral lineshapes are independent of $i \pm 3$ and $i \pm 4$ mutations to alanine.[19,25] In light of this, Columbus et al.[5] and Liang et al.[16] hypothesized that the backbone mobility, which is different at these two sites because of their attachment to helices of different length and rigidity, is responsible for the line shape difference at these two sites. Site 72 is located in the middle of a long 5-turn helix and is thought to be one of the most highly ordered helical surface sites.[5,16,19] Site 131 is on a short 2.5-turn helix and is more flexible in terms of higher Debye−Waller factors and hydrogen exchange rates when compared to site 72.[5] Tombolato et al. found that the spectra of 131R1 could not be simply obtained by adjusting the populations of the three components obtained from the simulation of 72R1′s spectra. (They developed their theoretical model only for the 72 site and not for the 131 site.) Thus they postulated that the backbone dynamics is most likely the main reason for the observed difference between the spectra of 72R1 and 131R1, supporting the hypothesis suggested by Columbus et al. and Liang et al.[5,16] It was noted by Columbus et al.[5] that the immobile component, which is common in the spectra of both R1 and R2, most likely arises from the interactions of the nitroxide ring with the protein surface. Thus, it does not directly reflect the modulation of the internal motion by the backbone dynamics.[7] On the other hand, the conformers corresponding to the intermediate and the mobile components were modeled to have no interaction with the surrounding residues.[25] Thus, they can be used to infer the backbone motion.

R2 has been suggested by Columbus et al. to be a useful probe for the backbone dynamics because the steric clash of the 4-methyl group with the disulfide constrains rotations about the side chain bonds (e.g., χ_5), resulting in the enhanced sensitivity to the backbone dynamics.[5] Since the mobility of R2 is restricted by interaction within the side chain itself rather than by interaction with its local environment, R2 can be used to monitor the backbone dynamics even more readily than R1.[5]

Our results show that for the intermediate component of R2 the values of S_{20} at the two sites of 72 and 131 are similar. However, for both the intermediate and the mobile components of R1 the values of S_{20} at the two sites are significantly different. This result raises the question whether the backbone dynamics does account for the spectral difference at the two sites or whether R1 and R2 can both be used to probe the backbone dynamics. Sezer et al. found from their molecular dynamics simulations that the most populated conformers of 72R1 are well localized, and in contrast the most populated conformers of 131R1 are more diffuse.[24] Taken together, our results suggest that the backbone motion might not be the major contributor to the line shape difference at these two sites, if we take as given the assumption that R2 can probe the backbone mobility. It is however possible that the conformers corresponding to the intermediate component of R2 have some interactions with the local environment. If this were the case, then the differences in the ESR spectra of 72R1 and 131R1 might well be reflecting the differences in their backbone motion as suggested by Columbus et al. and Tombolato et al.[5,22] It should be noted that the differences in order parameters for the dominant component at these two sites corresponds to only ∼5° in average angular amplitude.

However for 72R2 versus 131R2, the S_{20} values for the "intermediate" component are similar, a result that might not be expected if the difference between the sites is due to backbone motions. It is self-evident that the motion of R1 will reflect particular modes of backbone flexibility on the ns time scale. For example, the studies of Columbus et al. clearly revealed the highly flexible backbone segments of GCN4[7] that were previously identified by NMR relaxation. Hence, SDSL will be a powerful tool in identifying "disordered" domains in proteins using a similar approach. However, uncertainty remains as to the origin of relatively small differences in R1 motion, such as that between 72R1 and 131R1.

Effects of Ficoll. Sucrose solutions (30 w/w%) in which R^{c} of T4L is reduced by about a factor of 3 at room temperature, has been used to increase the viscosity of the solution and minimize the contribution of R^{c} to the 9 GHz spectral line shape.[19,41,42] Under such conditions the 9 GHz spectra of T4L can be analyzed using the MOMD model. In the present study, we used Ficoll 70 instead of sucrose as the viscogen to slow the global tumbling of the protein, because Ficoll does not produce effects of preferential hydration characteristic of

sucrose.[41] As shown in Figure 8, the microscopic viscosity of 25 w/v % Ficoll solution relative to that in an aqueous solution is 3.33 on average for the three samples at room temperature. This means that R^c is reduced in 25% Ficoll solution to about the same level as in 30% sucrose solution, as found by Lopez et al.[41]

We are now able to test whether the contribution of R^c in 25% Ficoll solution to the 9 GHz spectra of T4L is really negligible, given that the global tumbling and the internal motion are explicitly included in the simulations using the SRLS model. We chose 72R2 as the example. 9 GHz and 170 GHz spectra were simulated with the best fit parameters from the fits to the multifrequency spectra of 72R2 in 25 w/v % Ficoll solution at 22 °C (see Supporting Information Table 2), except for the value of R^c in Supporting Information Figure 5. It is seen in Supporting Information Figure 5 that whereas R^c in 25% Ficoll solution is not strictly in the rigid limit, it is slow enough that it hardly contributes to line shape of the 9 GHz spectrum. (This observation is sensitive to the angle β_d used in the simulation for reasons noted in Results: Part 1, Subsection 5; thus, when a $\beta_d = 0°$ is used, the overall tumbling has a greater effect on the line shape).

We noted in Results that Ficoll has some effect on the internal motion of the immobile component of R2. We further demonstrate the Ficoll effect in Figure 12. The solid line spectrum was simulated with the best fit parameters from the fits to the multifrequency spectra in water solution at 22 °C (see Supporting Information Table 1), except that R^c was set to the best fit value in 25% Ficoll solution (see Supporting Information Table 2). The dashed line spectrum was simulated with the best fit parameters from the fits to the multifrequency spectra in 25% Ficoll solution at 22 °C (see Supporting Information Table 2). The difference between the two simulated spectra in Figure 12A,B,C respectively show Ficoll's effect on the internal motion of 72R2, 131R2, and 131R1.

For 72R2 and 131R2 (see Figure 12A,B), the difference at 9 GHz is small (see also ref 41) but the difference at high frequency is prominent. A reduction in $R^o_\perp$ of the immobile component contributes most to the prominent line shape change at high frequency caused by adding Ficoll. The three peaks in the g_{zz} region of the 170 GHz spectrum of 72R2 or the 240 GHz spectrum of 131R2 are from the immobile component and shift dramatically to the high field direction with Ficoll in the solution, confirming that the high field ESR is more sensitive in observing any change in the immobile component. The fact that the 9 GHz spectra are much less sensitive to the immobile component, and it is this component rather than the intermediate one, that is affected by the Ficoll (cf. Figure 9) may explain why the addition of sucrose up to 40 w/w% appears to have no effect on the internal motion, as concluded from the simple analysis of the 9 GHz spectra.[33,41] If the focus is on just the intermediate component then it follows from Figure 9, that the addition of Ficoll hardly affects its motion. However, adding Ficoll increases the ordering of the intermediate component by 0.01−0.05.

For 131R1 (see Figure 12C), the difference at 9 GHz is even smaller compared to the two cases for R2. The very little change in the 9 GHz spectrum is consistent with what Lopez et al. concluded from their extensive 9 GHz study on R1 that Ficoll has little effect on the internal motion of the spin label.[41] However, although the difference at 9 GHz is almost negligible, we still observe some difference at 240 GHz caused by the changes in $R^o_\perp$ and the ordering of the mobile and intermediate components.

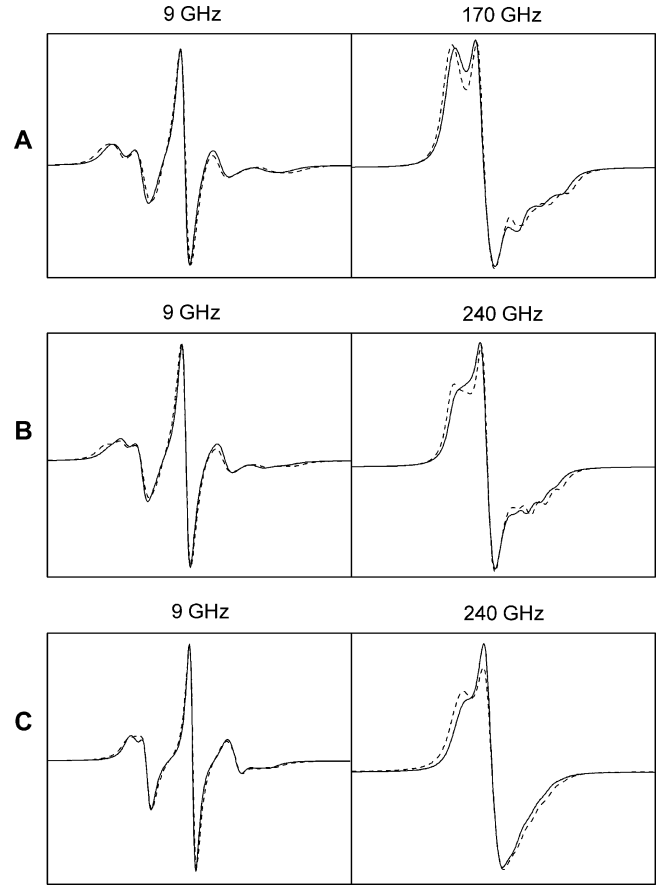

Figure 12. Comparison of two 9 (170 or 240) GHz simulated spectra with the dynamic and ordering parameters of the internal motion set to values in water solution (solid lines) and in 25 w/v % Ficoll solution (dashed lines) respectively. The solid line spectra were simulated with the best fit parameters at 22 °C in water solution (see Supporting Information Table 1), except that R^c was set to the value in 25 w/v % Ficoll solution (see Supporting Information Table 2): (A) 72R2; (B) 131R2; and (C) 131R1. The dashed line spectra were simulated with the best fit parameters at 22 °C in 25 w/v % Ficoll solution (see Supporting Information Table 2).

What then is the mechanism by which Ficoll slows down the internal motion? There are two relevant ones that one may consider, both based on the well-known molecular crowding properties of Ficoll 70.[43] First, for proteins that occupy a manifold of conformational states, each with a different volume, crowders will drive the equilibrium toward the state of minimum volume. T4L is a two-domain protein with interdomain hinges that allow opening and closing of the active site cleft.[44] The open state is the dominant population in solution,[45,46] and has a larger excluded volume than the closed state. As anticipated, Ficoll 70 (25% w/w) drives the equilibrium toward the closed state.[47] On the other hand, the melting point of T4L is insensitive to Ficoll 70,[41] and the C terminal domain in which 72 and 131 reside is very stable,[48] characterized by low Debye−Waller factors in the crystal structures,[49] and shows no detectable conformational exchange in NMR relaxation experiments.[39] Thus, there is no evidence for substantial conformational heterogeneity in the C terminal domain that would be modulated by a crowder. Moreover, the 9 GHz spectrum of 72R1 is apparently insensitive to the hinge motion,[45] as is 131R1.[50] Collectively, these data make it unlikely that Ficoll 70 produces stabilization and increased packing of the T4L C terminal domain, in agreement with the lack of effect of Ficoll 70 on the internal motion of 72R1 and 131R1 observed here and in

the earlier study of Lopez et al.[41] Thus, one would also expect Ficoll 70 not to influence the motion of R2 at either site, contrary to the experimental data.

A second characteristic of crowders is the ability to drive intermolecular associations that would not normally be observed, that is, the formation of oligomers. T4L is clearly monomeric in solution at low concentrations, but at the high concentrations needed in these experiments (1−2 mM) in the presence of 25% w/w Ficoll 70 with a fractional volume occupation of ca. 60%[43] it is entirely possible that weak and nonspecific surface associations occur between T4L molecules or between T4L and Ficoll 70. If this is the case, our results could be explained by assuming that the more hydrophobic R2 is instrumental in driving the association, and hence the crowder only influences T4L molecules bearing R2 and not R1.

Overall Assessment

We wish now to make an overall assessment of this study and its implications. Clearly the multifrequency approach provides substantial information to study the complex dynamics of a protein such as T4L. Not only do the different frequency spectra supply "snapshots" at different time-scales of the dynamics, (i.e., higher frequencies give faster time-scale insights and lower frequencies slower ones), but they also provide "snapshots from different angles". That is, the lower frequency spectra are mostly influenced by the nearly axially symmetric hyperfine tensor, for which the z-component is dominant, whereas the high frequency spectra are most influenced by the fully asymmetric **g** tensor wherein both the x and z components differ substantially from its trace. Thus, whereas motion about an axis parallel to the magnetic z-axis is difficult to discern at 9 GHz, it is very clear at the high frequencies, as are motions relative to the other magnetic axes.[51] Taken together, these features emphasize the value of the multifrequency approach to study molecular dynamics.

On the other hand, when dealing with dynamics as complex as displayed in the present study on T4L, the substantial independent experiments provided in this study are not in themselves guarantors of sufficient information to disentangle all the complex features. This is a primary reason that we analyzed the data in the context of what we refer to as a "mesoscopic" model, viz. the SRLS model. The SRLS model, which distinguishes internal and overall motions but does allow for several components, already provides numerous parameters to fit to the experimental spectra. We have found it necessary to restrict somewhat the parameters that we chose to fit, hopefully in a reasonable manner, as we have discussed above. Clearly, further efforts at improving the model for fitting these spectra would be of value, but one must be wary of introducing too many fitting parameters. Recent efforts at improved models include that of Tombolato et al.,[22] which adds an atomistic viewpoint to the SLE, and the fully atomistic viewpoint provided by the MD study of Sezer et al.[24]

Experimental studies clearly reveal the role of internal motion of the R1 side chain in determining the ESR spectra.[5,19] The R1 internal motion presents a difficulty in extracting information on backbone dynamics on the same time scale, and new strategies are needed. An obvious approach is to design new spin label side chains with highly restricted internal motion. Alternatively, backbone dynamic modes can be selectively excited by cavity-creating or overpacking mutations at a distance from the label site. Efforts in both directions are currently under study. In combination with the very significant ability of the multifrequency ESR method to clearly distinguish internal motions from the slower overall motions, one may expect significant future progress in the study of protein dynamics by these ESR methods.

We would now like to address a specific issue that arises in using multifrequency data to fit to the dynamical model utilized. One can, in general, fit an individual single frequency spectrum with somewhat higher quality of fit and perhaps fewer parameters than emerges in the fitting of as many as four different spectra all at different frequencies. However, given what we have just noted, the spectra at the different frequencies provide different perspectives on the molecular motions, and therefore taken together provide a fuller picture of the dynamics, so they should all be given significant weight. It may be easy to obscure certain details of the dynamics from a single "snapshot" with a single "view-point" that may be observable from another. However, given that the model (e.g., the SRLS model that we have used) is an approximate one, then it will necessarily not include all the motional details that could affect the various ESR spectra (as we have argued above). It can therefore be expected that the snapshots taken at different speeds and view-points will uncover some details not well represented in the approximate model. This is a likely reason why we can generally fit individual spectra (each with their more limited information content) better than we do with the multifrequency approach. However, we do wish to emphasize that despite this fact, a major achievement in the present study is that we consistently do achieve good fits at all frequencies with the same set of fitting parameters. Further progress in assessing the relative importance of the features in the spectra at each frequency would benefit from careful sensitivity analysis, as is currently being conducted by Earle et al.[52]

Conclusions

(1) Best global fits to a SRLS model using data from four frequencies on T4 lysozyme in aqueous solution over a temperature range of 2−32° require three spectral components characterized as relatively "mobile", "intermediate", and "immobile" for both 72R1 and 131R1. In the case of 72R2 and 131R2 only the intermediate and immobile components are found.

(2) In all cases, for the spectra at all four frequencies, very good simultaneous fits were achieved at all temperatures with the SRLS model.

(3) The immobile component is highly ordered and slower in its motion and is more populated in the R2 spectra. This component may correspond to conformers stabilized by interaction with the protein surface.

(4) The mobile and intermediate components exhibit fast anisotropic local diffusion and relatively low ordering. They most likely correspond to conformers having little or no interactions with nearby residues.

(5) The more mobile components of 72R1 and 131R1 exhibit significantly different S_{20} values, with that for 72R1 being significantly greater, as is consistent with previous studies that suggested that this difference results from reduced backbone flexibility for 72R1.

(6) The **g** tensor and hyperfine tensor for all four spin-labeled mutants measured from rigid-limit multifrequency spectra (in low temperature viscous sucrose/water solution) are identical within experimental uncertainty indicating they are all in very similar polarity environments.

(7) The values for overall tumbling rate, R^c, obtained independently from each of the four spin-labeled mutants were generally in very good agreement with each other and agree favorably with estimates from NMR and hydrodynamic modeling. This supports the results of the SRLS analysis.

(8) The addition of Ficoll reduces R^c according to a microscopic viscosity that is proportional to the macroscopic viscosity taken to the 0.39 power, and reduces substantially the motional rate of the immobile component in R2, but has much less effect on the intermediate component of 72R2 and 131R2 and the three components of 131R1.

Acknowledgment. This project was supported by Grant 5P41RR016292 (J.H.F) from the National Center for Research Resources (NCRR), a component of the National Institutes of Health (NIH), and by National Institutes of Health Grants R01EY05216 (W.L.H), RT32EY007026 (M.R.F.) and the Jules Stein Professor endowment (W.L.H.).

Supporting Information Available: They include the fitting procedure for determining magnetic tensor components; details on the global nonlinear least-squares (NLLS) fitting; best fit parameters in aqueous and in Ficoll solutions; the two versus three component fits to spectra of 131R1 and single-component fits to spectra of R2; variation of the reduced χ^2 with the diffusion tilt angle; further discussion of spectra recorded in 65% sucrose solution; contribution of the global tumbling in 25% Ficoll solution. This material is available free of charge via the Internet at http://pubs.acs.org.

References and Notes

(1) Hubbell, W. L.; Mchaourab, H. S.; Altenbach, C.; Lietzow, M. A. Watching Proteins Move using Site-Directed Spin Labeling. *Structure* **1996**, *4*, 779–783.

(2) Hubbell, W. L.; Gross, A.; Langen, R.; Lietzow, M. A. Recent Advances in Site-Directed Spin Labeling of Proteins. *Curr. Opin. Struct. Biol.* **1998**, *8*, 649–656.

(3) Hubbell, W. L.; Cafiso, D. S.; Altenbach, C. Identifying Conformational Changes with Site-Directed Spin Labeling. *Nat. Struct. Biol.* **2000**, *7*, 735–739.

(4) Borbat, P. P.; Costa-Filho, A. J.; Earle, K. A.; Moscicki, J. K.; Freed, J. H. Electron Spin Resonance in Studies of Membranes and Proteins. *Science* **2001**, *291*, 266–269.

(5) Columbus, L.; Kalai, T.; Jeko, J.; Hideg, K.; Hubbell, W. L. Molecular Motion of Spin Labeled Side Chains in Alpha-Helices: Analysis by Variation of Side Chain Structure. *Biochemistry* **2001**, *40*, 3828–3846.

(6) Columbus, L.; Hubbell, W. L. A New Spin on Protein Dynamics. *Trends Biochem. Sci.* **2002**, *27*, 288–295.

(7) Columbus, L.; Hubbell, W. L. Mapping Backbone Dynamics in Solution with Site-Directed Spin Labeling: GCN4−58 bZip Free and Bound to DNA. *Biochemistry* **2004**, *43*, 7273–7287.

(8) Fanucci, G. E.; Cafiso, D. S. Recent Advances and Applications of Site-Directed Spin Labeling. *Curr. Opin. Struct. Biol.* **2006**, *16*, 644–653.

(9) Dalton, L. In *EPR and Advanced EPR Studies of Biological Systems*; Dalton, L., Ed.; CRC Press: Boca Raton, FL, 1985; Chapter 1, pp 1−10.

(10) Berliner, L. J. Spin Labeling: the Next Millenium. In *Biological Magnetic Resonance*; Berliner, L. J., Ed.; Plenum: New York, 1998; Vol. 14.

(11) Budil, D. E.; Earle, K. A.; Freed, J. H. Full Determination of the Rotational Diffusion Tensor by Electron Paramagnetic Resonance at 250 GHz. *J. Phys. Chem.* **1993**, *97*, 1294–1303.

(12) Liang, Z.; Freed, J. H. An Assessment of the Applicability of Multifrequency ESR to Study the Complex Dynamics of Biomolecules. *J. Phys. Chem. B* **1999**, *103*, 6384–6396.

(13) Freed, J. H. New Technologies in Electron Spin Resonance. *Annu. Rev. Phys. Chem.* **2000**, *51*, 655–689.

(14) Barnes, J. P.; Liang, Z.; Mchaourab, H. S.; Freed, J. H.; Hubbell, W. L. A Multifrequency Electron Spin Resonance Study of T4 Lysozyme Dynamics. *Biophys. J.* **1999**, *76*, 3298–3306.

(15) Poluektov, O. G.; Utschig, L. M.; Dalosto, S.; Thurnauer, M. C. Probing Local Dynamics of the Photosynthetic Bacterial Reaction Center with a Cysteine Specific Spin Label. *J. Phys. Chem. B* **2003**, *107*, 6239–6244.

(16) Liang, Z.; Lou, Y.; Freed, J. H.; Columbus, L.; Hubbell, W. L. A Multifrequency Electron Spin Resonance Study of T4 Lysozyme Dynamics using the Slowly Relaxing Local Structure Model. *J. Phys. Chem. B* **2004**, *108*, 17649–17659.

(17) White, G. F.; Ottignon, L.; Georgiou, T.; Kleanthous, C.; Moore, G. R.; Thomson, A. J.; Oganesyan, V. S. Analysis of Nitroxide Spin Label Motion in a Protein-Protein Complex using Multiple Frequency EPR Spectroscopy. *J. Magn. Reson.* **2007**, *185*, 191–203.

(18) Nesmelov, Y. E.; Karim, C. B.; Song, L.; Fajer, P. G.; Thomas, D. D. Rotational Dynamics of Phospholamban Determined by Multifrequency Electron Paramagnetic Resonance. *Biophys. J.* **2007**, *93*, 2805–2812.

(19) Mchaourab, H. S.; Lietzow, M. A.; Hideg, K.; Hubbell, W. L. Motion of Spin-Labeled Side Chains in T4 Lysozyme. Correlation with Protein Structure and Dynamics. *Biochemistry* **1996**, *35*, 7692–7704.

(20) Polimeno, A.; Freed, J. H. Slow Motional ESR in Complex Fluids: The Slowly Relaxing Local Structure Model of Solvent Cage Effects. *J. Phys. Chem.* **1995**, *99*, 10995–11006.

(21) Budil, D. E.; Sale, K. L.; Khairy, K. A.; Fajer, P. G. Calculating Slow-Motional Electron Paramagnetic Resonance Spectra from Molecular Dynamics using a Diffusion Operator Approach. *J. Phys. Chem. A* **2006**, *110*, 3703–3713.

(22) Tombolato, F.; Ferrarini, A.; Freed, J. H. Modeling the Effects of Structure and Dynamics of the Nitroxide Side Chain on the ESR Spectra of Spin-Labeled Proteins. *J. Phys. Chem. B* **2006**, *110*, 26260–26271.

(23) Fleissner, M. R. Ph.D. Thesis, University of California, Los Angeles, CA, 2007.

(24) Sezer, D.; Freed, J. H.; Roux, B. Multifrequency Electron Spin Resonance Spectra of a Spin-Labeled Protein Calculated from Molecular Dynamics Simulations. *J. Am. Chem. Soc.* **2009**, *131*, 2597–2605.

(25) Fleissner, M. R.; Cascio, D.; Hubbell, W. L. Structural Origin of Weakly Ordered Nitroxide Motion in Spin-Labeled Proteins. *Protein Sci.* **2009**, *18*, 893–908.

(26) Hofbauer, W.; Earle, K. A.; Dunnam, C. R.; Moscicki, J. K.; Freed, J. H. A High-Power 95 GHz Pulsed Electron Spin Resonance Spectrometer. *Rev. Sci. Instrum.* **2004**, *75*, 1194–1208.

(27) Earle, K. A.; Dzikovski, B.; Hofbauer, W.; Moscicki, J. K.; Freed, J. H. High-Frequency ESR at ACERT. *Magn. Reson. Chem.* **2005**, *43*, S256–66.

(28) Barnes, J. P.; Freed, J. H. Aqueous Sample Holders for High Frequency Electron Spin Resonance. *Rev. Sci. Instrum.* **1997**, *68*, 2838–2846.

(29) Earle, K. A.; Budil, D. E.; Freed, J. H. 250-GHz EPR of Nitroxides in the Slow-Motional Regime: Models of Rotational Diffusion. *J. Phys. Chem.* **1993**, *97*, 13289–13297.

(30) Budil, D. E.; Earle, K. A.; Lynch, W. B.; Freed, J. H. Electron Paramagnetic Resonance at 1 millimeter Wavelengths. In *Advanced EPR: Applications in Biology and Biochemistry*; Hoff, A., Ed.; Elsevier; Amsterdam, 1989; Chapter 8, pp307−340.

(31) Ablett, S.; Izzard, M. J.; Lillford, P. J. Differential Scanning Calorimetric Study of Frozen Sucrose and Glycerol Solutions. *J. Chem. Soc. Faraday Trans.* **1992**, *88*, 789–794.

(32) Roozen, M.; J, G. W.; Hemminga, M. A. Molecular Motion in Sucrose-Water Mixtures in the Liquid and Glassy State as Studied by Spin Probe ESR. *J. Phys. Chem.* **1990**, *94*, 7326–7329.

(33) Timofeev, V. P.; Tsetlin, V. I. Analysis of Mobility of Protein Side Chains by Spin Label Technique. *Eur. Biophys. J.* **1983**, *10*, 93–108.

(34) Budil, D. E.; Lee, S.; Saxena, S.; Freed, J. H. Nonlinear-Least-Squares Analysis of Slow-Motion EPR Spectra in One and Two Dimensions using a Modified Levenberg-Marquardt Algorithm. *J. Magn. Reson., Ser. A* **1996**, *120*, 155–189.

(35) Ondar, M. A.; Grinberg, O. Y.; Dubinskii, A. A.; Lebedev, Y. S. Study of the Effect of the Medium on the Magnetic-Resonance Parameters of Nitroxyl Radicals by High-Resolution EPR Spectroscopy. *Sov. J. Chem. Phys.* **1985**, *3*, 781–792.

(36) Earle, K. A.; Moscicki, J. K.; Ge, M.; Budil, D. E.; Freed, J. H. 250-GHz Electron Spin Resonance Studies of Polarity Gradients Along the Aliphatic Chains in Phospholipid Membranes. *Biophys. J.* **1994**, *66*, 1213–1221.

(37) McConnell, H. M.; McFarland, B. G. Physics and Chemistry of Spin Labels. *Q. Rev. Biophys.* **1970**, *3*, 91–136.

(38) Snipes, W.; Cupp, J.; Cohn, G.; Keith, A. Electron Spin Resonance Analysis of the Nitroxide Spin Label 2,2,6,6-Tetramethylpiperidone-N-Oxyl (Tempone) in Single Crystals of the Reduced Tempone Matrix. *Biophys. J.* **1974**, *14*, 20–32.

(39) Mulder, F. A.; Hon, B.; Mittermaier, A.; Dahlquist, F. W.; Kay, L. E. Slow Internal Dynamics in Proteins: Application of NMR Relaxation Dispersion Spectroscopy to Methyl Groups in a Cavity Mutant of T4 Lysozyme. *J. Am. Chem. Soc.* **2002**, *124*, 1443–1451.

(40) Lavalette, D.; Tetreau, C.; Tourbez, M.; Blouquit, Y. Microscopic Viscosity and Rotational Diffusion of Proteins in a Macromolecular Environment. *Biophys. J.* **1999**, *76*, 2744–2751.

(41) Lopez, C. J.; Fleissner, M. R.; Guo, Z.; Kusnetzow, A. K.; Hubbell, W. L. Osmolyte Perturbation Reveals Conformational Equilibria in Spin-Labeled Proteins. *Protein Sci.* **2009**, *18*, 1637–1652.

(42) Guo, Z.; Cascio, D.; Hideg, K.; Hubbell, W. L. Structural Determinants of Nitroxide Motion in Spin-Labeled Proteins: Solvent-Exposed Sites in Helix B of T4 Lysozyme. *Protein Sci.* **2008**, *17*, 228–239.

(43) Wenner, J. R.; Bloomfield, V. A. Crowding Effects on EcoRV Kinetics and Binding. *Biophys. J.* **1999**, *77*, 3234–3241.

(44) Faber, H. R.; Matthews, B. W. A Mutant T4 Lysozyme Displays Five Different Crystal Conformations. *Nature* **1990**, *348*, 263–266.

(45) Mchaourab, H. S.; Oh, K. J.; Fang, C. J.; Hubbell, W. L. Conformation of T4 Lysozyme in Solution. Hinge-Bending Motion and

the Substrate-Induced Conformational Transition Studied by Site-Directed Spin Labeling. *Biochemistry* **1997**, *36*, 307–316.

(46) Goto, N. K.; Skrynnikov, N. R.; Dahlquist, F. W.; Kay, L. E. What is the Average Conformation of Bacteriophage T4 Lysozyme in Solution? A Domain Orientation Study using Dipolar Couplings Measured by Solution NMR. *J. Mol. Biol.* **2001**, *308*, 745–764.

(47) Lopez, C. J.; Fleissner, M. R.; Hubbell, W. L. University of California, Los Angeles, CA. Unpublished work, 2009.

(48) Cellitti, J.; Llinas, M.; Echols, N.; Shank, E. A.; Gillespie, B.; Kwon, E.; Crowder, S. M.; Dahlquist, F. W.; Alber, T.; Marqusee, S. Exploring Subdomain Cooperativity in T4 Lysozyme I: Structural and Energetic Studies of a Circular Permutant and Protein Fragment. *Protein Sci.* **2007**, *16*, 842–851.

(49) Weaver, L. H.; Matthews, B. W. Structure of Bacteriophage T4 Lysozyme Refined at 1.7 A Resolution. *J. Mol. Biol.* **1987**, *193*, 189–199.

(50) Fleissner, M. R.; Altenbach, C.; Hubbell, W. L. University of California, Los Angeles, CA. Unpublished work, 2009.

(51) Dzikovski, B.; Tipikin, D.; Livshits, V.; Earle, K.; Freed, J. Multifrequency ESR Study of Spin-Labeled Molecules in Inclusion Compounds with Cyclodextrins. *Phys. Chem. Chem. Phys.* **2009**, *11*, 6676–6688.

(52) Earle, K. A.; Mainalli, L.; Sahu, I. D.; Schneider, D. J. Magnetic Resonance Spectra and Statistical Geometry. *Appl. Magn. Reson.* **2010**, *37*, 865–880.

JP910606H